International Journal of Solids and Structures 191–192 (2020) 614–627

Contents lists available at ScienceDirect

International Journal of Solids and Structures

journal homepage: www.elsevier.com/locate/ijsolstr

Dynamics of variable length geometrically exact beams in three-dimensions

Nikhil Singh, Ishan Sharma*, Shakti Singh Gupta

NL-213, IIT Kanpur, Kanpur India

ARTICLE INFO

Article history:
Received 7 December 2018
Revised 31 October 2019
Accepted 5 November 2019
Available online 22 November 2019

Keywords:
Geometrically exact beam theory
GEBT
Dynamics
FEM
Variable length GE beam
Finite element method

ABSTRACT

We investigate the three-dimensional dynamics of a variable-length, geometrically-exact beam. The beam is released / retracted from a guide. Geometrically exact beam theory, like regular beam theory, is phrased in terms of the deformation of a neutral axis and the rotations of the cross-sections normal to the neutral axis. In contrast to beams in linear elasticity, geometrically exact beams allow large rotations of the beam's cross-section and large deformations of the line of centroids. We derive the necessary governing equations for the system which, in three dimensions, contain non-trivial contributions from three-dimensional rotations coupled to the varying length of the cable. These equations are then solved through a Galerkin finite element method, after first mapping the physical domain to a fixed computational domain. Large rotations are incorporated into the finite element procedure by utilizing the exponential representation of the rotation tensor. Finally, as an important application of our computational formulation, we investigate the three-dimensional dynamics of a spinning, vibrating, variable-length, flexible beam through a sequence of increasingly complex examples.

1. Introduction

Engineering of moving flexible structures finds its application in various areas of engineering, such as robotics, air to air refuelling, deployment of aerostats and conveyor belts. In many of these applications the extent of deformation is large, and the contribution of shear stresses on the deformation is not negligible. Thus, cross-sections can deform, rotate by a large amount, and may not remain normal to the neutral axis. At the same time, the strain magnitudes can still be small, so that a fully nonlinear three-dimensional analysis may not be necessary. Indeed, the aforementioned aspects are successfully captured by the Geometrically Exact Beam Theory (GEBT) introduced by Reissner (1973) and popularized by Simo (1985), and other generalized beam theories such as those given in Antman (1974), Green et al. (1974), etc. The above references present beam formulations but do not show their numerical implementations.

The GEBT with shear deformation has been implemented in various research works over the years (Vu-Quoc and Simo, 1987; Simo and Vu-Quoc, 1988; Vu-Quoc, 1986; Simo and Vu-Quoc, 1986; Ibrahimbegović, 1995). Some of the recent applications of GEBT can be found in Rubin (2001), Cao et al. (2006), Friedmann et al. (2009), Liu and Lu (2016). In a special version of GEBT the cross-sections do not change shape, but are allowed to rotate in three-dimensions, as in Vu-Quoc and Simo (1987), Simo and Vu-Quoc (1988), Simo and Vu-Quoc (1986), Vu-Quoc (1986). Preceding references make use of differential topology for the formulation of finite rotations and their derivatives. McRobie and Lasenby (1999) recently presented a different approach using geometric algebra. They presented a reformulation of the rotation inertia term in Simo and Vu-Quoc (1986) but did not provide any numerical examples.

Humer (2013) investigate the planar dynamics of a slender beam sliding through an orifice which is fixed in space. The work makes use of a non-linear beam formulation accounting for large vibrations but neglecting the effects of shear and rotatory inertia of the cross-section. Vu-Quoc and Li (1995) extended GEBT with shear deformation to address situations wherein the beam's length varies, but limited themselves to the planar situation. Steinbrecher et al. (2017) present a comparison of different numerical approaches for the planar sliding beam problem by providing solutions using conventional planar elasticity and Reissner's beam theory. The authors also discuss the implementation of contact formulations to impose proper boundary conditions. To simulate the sliding-beam formulation the authors use an open-source simulation software HOTINT (Gerstmayr et al., 2013). The references on the sliding beam problems above confine themselves to the planar case, however, engineering applications typically in-

* Corresponding author.
E-mail address: ishans@iitk.ac.in (I. Sharma).

https://doi.org/10.1016/j.ijsolstr.2019.11.005
0020-7683/

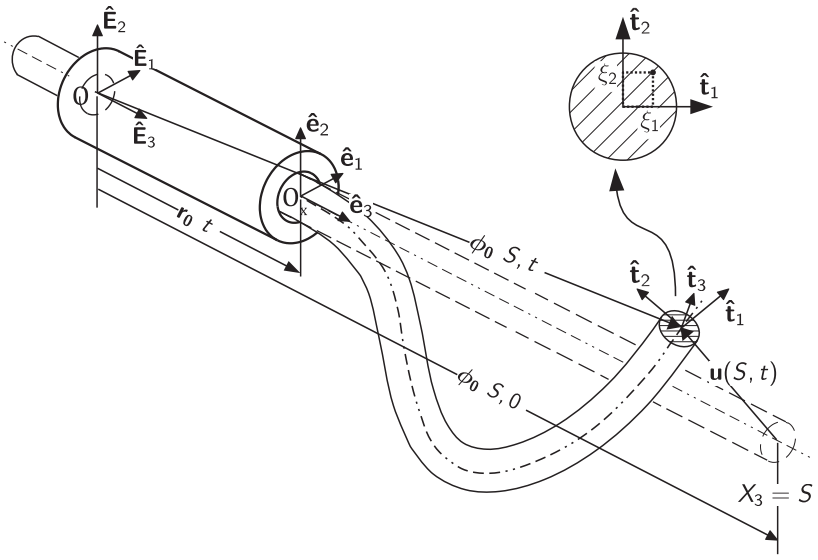

Fig. 1. Sketch of the reference (undeformed) and current (deformed) configurations of a variable length, flexible GE beam in three dimensions.

volve three-dimensional deformation, and this motivates the current study of three-dimensional deformations of variable length GE beams. We will derive the governing equations, and then develop a computational algorithm based on the Finite Element (FE) method to solve those equations. The algorithm is validated by comparing with several benchmark problems and checking for conservation of angular momenta. Finally we demonstrate the utility of the three-dimensional, varying length GE beam theory by solving several, increasingly complex, examples.

In Section 2.1 we describing the kinematics of the system under specified assumptions. Utilizing the results of Section 2.1, we establish the governing equations for the system in Sections 2.2 and 2.3. Section 2.4 describes forces in terms of material vector fields using a pull back strategy. In Section 2.5 we discuss the mapping of the physical domain to a fixed computational domain. Section 3 discusses the finite element formulation for the problem described in Section 2. Section 3.1 describes the admissible variation for the system which is followed by description of the weak form in Section 3.2 and its subsequent linearization in Sections 3.3 and 3.4. In Section 4 we demonstrate the three-dimensional dynamics of the beam using various problems.

2. Algebraic formulation

Deflection of beams can be decomposed into (a) deformation of a central axis of the beam defined in some suitable manner, e.g. the neutral axis, and (b) rotation and deformation of beam cross-sections that were normal to the central axis at some instant, say at the beginning of the deformation. A special formulation of Geometrically Exact (GE) beam theory enables us to solve problems involving large deformations of the central axis and large rotations of the cross-section, while making the following assumptions:

(a) plane cross-sections rotate rigidly during deformation, and
(b) deformation, although large, remains in the elastic region.

We now derive the governing equations for variable length GE beam, whose one end moves in a straight and smooth guide while the other end is free. The material elements of the beam inside the guide undergo only translation and no rotation.

2.1. Kinematics

With the assumptions mentioned above, the configuration of a beam may be defined by specifying the orientation of the cross-sections and the position vector of the cross-section's centroid. The curve joining the centroids of the cross-sections will be referred to as the *line of centroids*.

The cross-sections themselves are defined in a natural way in the reference configuration, e.g. for a beam that is initially a long, slender cylinder, the cross-sections in the reference configuration are taken to be normal to the cylindrical beam's symmetry axis. Let $S \in [0, L] \subset \mathbb{R}$ be the arc length coordinate measured from a fixed point O on the beam that locates the centroid in the reference configuration. Let point O be attached to the rod inside the guide, far from the guide's exit, which acts as the origin for the translating frame $\hat{\boldsymbol{E}}_i$. The $\hat{\boldsymbol{E}}_i$ frame can be accelerating making it necessary to define a separate spatially fixed frame defined by $\hat{\boldsymbol{e}}_i$, centred at the point O_X that is fixed at the opening of the guide. Fig. 1 shows a three-dimensional schematic of the system.

We define the map $\boldsymbol{\phi}_0(S, t)$ which generates the line of centroids in the current (deformed) configuration at any given time. Fig. 1 displays the vector $\boldsymbol{\phi}_0(S, 0)$ at the current time.

As initially plane cross-sections after deformation remain plane, their orientations may be defined using a normal vector $\hat{\boldsymbol{n}}$. Thus, the position of a point on the cross-section with centroid $\boldsymbol{\phi}_0(S, t)$ may be easily defined in an orthogonal frame $\{\hat{\boldsymbol{t}}_1(S, t), \hat{\boldsymbol{t}}_2(S, t), \hat{\boldsymbol{n}}(S, t)\}$, which will be referred to as the *moving frame*. For convenience, the notation $\hat{\boldsymbol{t}}_3(S, t) \equiv \hat{\boldsymbol{n}}(S, t)$ will be employed. The position vector for any point in the rod with respect to O in the deformed configuration is

$$\begin{aligned}\boldsymbol{\phi}_S(\xi_1, \xi_2, S, t) &= \boldsymbol{\phi}_0(S, t) + \sum_{i=1}^{2} \xi_i \hat{\boldsymbol{t}}_i(S, t) \\ &= \boldsymbol{\phi}_0(S, 0) + \boldsymbol{u}(S, t) + \sum_{i=1}^{2} \xi_i \hat{\boldsymbol{t}}_i(S, t), \end{aligned} \tag{2.1}$$

where $\xi_i \hat{\mathbf{t}}_i$ locates a material point on cross-section with respect to the cross-section's centroid; see inset in Fig. 1. Hence, the position vector of a material point with respect to O_X is

$$\boldsymbol{\varphi}(\xi_1, \xi_2, S, t) = \boldsymbol{\phi}_0(S, 0) + \boldsymbol{u}(S, t) - \boldsymbol{r}_0(t) + \sum_{i=1}^{2} \xi_i \hat{\mathbf{t}}_i(S, t), \tag{2.2}$$

where $\boldsymbol{r}_0(t)$ locates O_X with respect to O; see Fig. 1.

As the moving frame forms an orthogonal basis, there exists an orthogonal transformation $\underline{\boldsymbol{\Lambda}}(S)$ such that

$$\hat{\boldsymbol{t}}_i(S,t) = \underline{\boldsymbol{\Lambda}}(S,t)\cdot\hat{\boldsymbol{e}}_i. \tag{2.3}$$

In our case, the beam is initially straight, hence $\underline{\boldsymbol{\Lambda}}(S,0) = \underline{\mathbf{1}}$.

2.2. Linear and angular momenta

We now find expressions for linear and angular momenta of the beam. We first define time derivatives of the moving frame as

$$\dot{\hat{\boldsymbol{t}}}_i(S,t) = \dot{\underline{\boldsymbol{\Lambda}}}(S,t)\cdot\hat{\boldsymbol{e}}_i = \{\dot{\underline{\boldsymbol{\Lambda}}}(S,t)\cdot\underline{\boldsymbol{\Lambda}}^T(S,t)\}\cdot\hat{\boldsymbol{t}}_i = \underline{\boldsymbol{Q}}(S,t)\cdot\hat{\boldsymbol{t}}_i, \quad i=1,2,3\,. \tag{2.4}$$

where $\underline{\boldsymbol{Q}}(S,t) = \dot{\underline{\boldsymbol{\Lambda}}}(S,t)\cdot\underline{\boldsymbol{\Lambda}}^T(S,t)$ is a skew-symmetric tensor, with $\boldsymbol{w}(S,t)$ as the associated axial vector, so that

$$\dot{\hat{\boldsymbol{t}}}_i(S,t) = \boldsymbol{w}(S,t)\times\hat{\boldsymbol{t}}_i(S,t)\,. \tag{2.5}$$

The *linear momentum* per unit of reference length of a given cross-section A is given by

$$\boldsymbol{L}(S,t) = \int_A \rho_0(\xi,t)\dot{\boldsymbol{\varphi}}(\xi,S,t)d\xi = A_\rho(S)\{\dot{\boldsymbol{u}}(S,t) - \dot{\boldsymbol{r}}_0(t)\}, \tag{2.6}$$

where A_ρ is the mass per unit length in the reference configuration. In the above, we have employed (2.2), symmetry arguments and the fact that ξ_i are measured from the centroid of the cross-section.

The *angular momentum* per unit reference length of a given cross-section A can be evaluated in a similar fashion. The angular momentum about the centroid $\boldsymbol{\phi}_0(S,t)$ is given by

$$\begin{aligned}\boldsymbol{H}(S,t) &= \int_A \rho_0(\xi,S)\big[\boldsymbol{\varphi}(\xi,S,t) - \{\boldsymbol{\phi}_0(S,t) - \boldsymbol{r}_0(t)\}\big]\times\dot{\boldsymbol{\varphi}}(\xi,S,t)d\xi\\ &= \left[\int_A \rho_0(\xi,S)\{\,||\boldsymbol{\phi}-\boldsymbol{\phi}_0||^2\underline{\mathbf{1}} + (\boldsymbol{\phi}-\boldsymbol{\phi}_0)\otimes(\boldsymbol{\phi}-\boldsymbol{\phi}_0)\,\}d\xi\right]\cdot\boldsymbol{w}(S,t)\\ &= \underline{\boldsymbol{I}}_\rho(S)\cdot\boldsymbol{w}(S,t),\end{aligned} \tag{2.7}$$

where $\underline{\mathbf{1}}$ is the identity tensor,

$$\underline{\boldsymbol{I}}_\rho = \left(\sum_{i=1}^{2}\sum_{j=1}^{2}\int_A \rho_0\xi_i\xi_j d\xi\right)(\delta_{ij}\underline{\mathbf{1}} - \boldsymbol{t}_i\otimes\boldsymbol{t}_j) \tag{2.8}$$

is the cross-section's moment of inertia tensor, defined in terms of the Krönecker delta δ_{ij}, and $\boldsymbol{w}(S,t)$ is a spatial vector, defined through (2.5), which is associated with the spin of the *moving frame*. As in (2.6), we have employed symmetry arguments and the fact that $\boldsymbol{\phi}_0(S,t)$ is the centroid of the cross-section to obtain (2.7). It is important to note that while the inertia tensor's matrix is independent of time in the *moving frame*, it will vary in the fixed coordinate system. The inertia tensor in the fixed frame is given by $\underline{\boldsymbol{J}}_\rho = \underline{\boldsymbol{\Lambda}}^T\cdot\underline{\boldsymbol{I}}_\rho\cdot\underline{\boldsymbol{\Lambda}}$.

2.3. Balance laws

We now derive the local form of the balance laws for a geometrically exact beam with variable length. The force and moment balance equations will be derived for an infinitesimal element of the material configuration. The free body diagram for an element is shown in Fig. 2.

Linear momentum balance for the element in Fig. 2 is given by

$$\boldsymbol{n}(b,t) - \boldsymbol{n}(a,t) + \int_a^b \bar{\boldsymbol{n}}(S,t)dS = \frac{\partial}{\partial t}\int_a^b \boldsymbol{L}(S,t)dS, \tag{2.9}$$

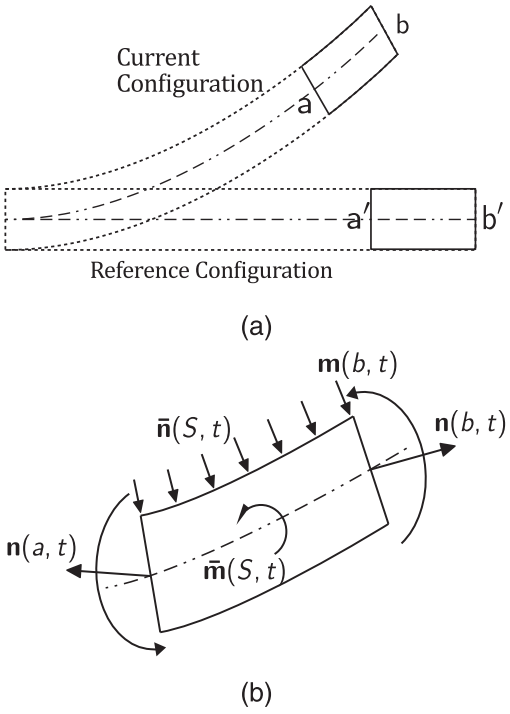

Fig. 2. (a) An element of the deformed beam in the reference and current configurations. (b) Free body diagram of the deformed element in (a).

where $\boldsymbol{n}(S,t)$ is the internal force acting on the cross-section S, $\bar{\boldsymbol{n}}(S,t)$ is the sum of external surface and body forces per unit reference length, and $\boldsymbol{L}(S,t)$ is the linear momentum per unit reference length defined by (2.6). Taking the limit b → a, dividing by the elemental length dS and using (2.6) yields the linear momentum balance

$$\frac{\partial\boldsymbol{n}(S,t)}{\partial S} + \bar{\boldsymbol{n}}(S,t) = A_\rho(S)\ddot{\boldsymbol{u}}(S,t) - A_\rho(S)\ddot{\boldsymbol{r}}_0(t)\,. \tag{2.10}$$

As the kinematic assumptions for the present formulation are the same as Vu-Quoc and Li (1995) and Simo (1985), therefore, the above equation when reduced to two dimensions matches the equation given by Vu-Quoc and Li (1995), and, matches the linear momentum balance given by Simo (1985), in case of a fixed length beam.

Angular momentum balance about point S=a is given by

$$\begin{aligned}&\boldsymbol{m}(b,t) - \boldsymbol{m}(a,t) + [\boldsymbol{\phi}_0(b,t) - \boldsymbol{\phi}_0(a,t)]\\ &\quad\times\boldsymbol{n}(b,t) + \int_a^b [\boldsymbol{\phi}_0(S,t) - \boldsymbol{\phi}_0(a,t)]\times\bar{\boldsymbol{n}}(S,t)\\ &\quad+\bar{\boldsymbol{m}}(S,t)dS = \frac{\partial}{\partial t}\int_a^b \boldsymbol{H}(S,t)dS,\end{aligned} \tag{2.11}$$

where $\boldsymbol{m}(S,t)$ is the internal moment, $\bar{\boldsymbol{m}}(S,t)$ is sum of external surface and body moment and $\boldsymbol{H}(S,t)$ is the angular momentum per unit of reference length defined by (2.7). Taking the limit b → a, dividing with elemental length dS, using (2.5), (2.7), (2.10) and (2.11) yields, finally,

$$\begin{aligned}&\frac{\partial\boldsymbol{m}(S,t)}{\partial S} + \frac{\partial\boldsymbol{\phi}_0(S,t)}{\partial S}\times\boldsymbol{n}(S,t) + \bar{\boldsymbol{m}}(S,t)\\ &\quad= \underline{\boldsymbol{I}}_\rho\cdot\dot{\boldsymbol{w}}(S,t) + \boldsymbol{w}(S,t)\times\left\{\underline{\boldsymbol{I}}_\rho(S)\cdot\boldsymbol{w}(S,t)\right\}\end{aligned} \tag{2.12}$$

The above matches the equation given by Simo (1985) and, in two-dimensions, reduces to the angular momentum balance given by Vu-Quoc and Li (1995).

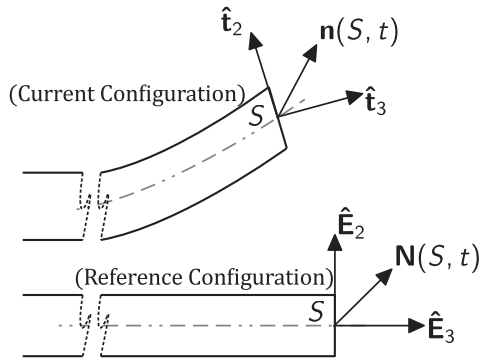

Fig. 3. Internal force in the reference and the current configurations.

2.4. Material description

The spatial vector and tensor fields $\boldsymbol{m}(S,t), \boldsymbol{n}(S,t), \underline{\boldsymbol{I}}_\rho(S)$, and $\boldsymbol{w}(S,t)$, are defined in terms of area elements of the deformed beam. Material vector and tensor fields are defined by *pulling back* these vector/tensor fields to the reference configuration through the orthogonal transformation $\underline{\boldsymbol{\Lambda}}(S,t)$:

$$\boldsymbol{n}(S,t) = \underline{\boldsymbol{\Lambda}}\cdot\boldsymbol{N}(S,t)\ ;\ \boldsymbol{m}(S,t) = \underline{\boldsymbol{\Lambda}}\cdot\boldsymbol{M}(S,t)\ ;\ \underline{\boldsymbol{I}}_\rho(S,t) = \underline{\boldsymbol{\Lambda}}\cdot\underline{\boldsymbol{J}}_\rho(S)\cdot\underline{\boldsymbol{\Lambda}}^T$$
$$\boldsymbol{w}(S,t) = \underline{\boldsymbol{\Lambda}}\cdot\boldsymbol{W}(S,t)\ ;\ \dot{\boldsymbol{w}}(S,t) = \underline{\boldsymbol{\Lambda}}\cdot\dot{\boldsymbol{W}}(S,t), \tag{2.13}$$

where $\boldsymbol{N}(S,t)$, $\boldsymbol{M}(S,t)$, $\underline{\boldsymbol{J}}_\rho(S)$ and $\boldsymbol{W}(S,t)$ are the material counterparts of $\boldsymbol{n}(S,t)$, $\boldsymbol{m}(S,t)$, $\underline{\boldsymbol{I}}_\rho(S,t)$ and $\boldsymbol{w}(S,t)$ respectively. The last of (2.13) is obtained by taking the time derivative of $\boldsymbol{w}(S,t)$ and employing (2.4) as follows:

$$\dot{\boldsymbol{w}}(S,t) = \dot{\underline{\boldsymbol{\Lambda}}}\cdot\boldsymbol{W}(S,t) + \underline{\boldsymbol{\Lambda}}\cdot\dot{\boldsymbol{W}}(S,t) = \underline{\boldsymbol{\Lambda}}\cdot\dot{\boldsymbol{W}}(S,t),$$

where, we recall from (2.4) that, $\underline{\boldsymbol{Q}}\cdot\boldsymbol{w} = \boldsymbol{w}\times\boldsymbol{w} = 0$.

We observe that the components of the vector fields $\boldsymbol{n}(S,t)$ and $\boldsymbol{m}(S,t)$ in the moving frame are the same as the components of the material vector fields $\boldsymbol{N}(S,t)$ and $\boldsymbol{M}(S,t)$ in the *fixed frame*, i.e. if $\boldsymbol{N} = N_i\hat{\boldsymbol{e}}_i$ and $\boldsymbol{M} = M_i\hat{\boldsymbol{e}}_i$ then $\boldsymbol{n} = N_i\hat{\boldsymbol{t}}_i$ and $\boldsymbol{m} = M_i\hat{\boldsymbol{t}}_i$.

Fig. 3 shows a schematic that explains spatial and material vectors using the example of $\boldsymbol{n}$ and $\boldsymbol{N}$.

The material description of the governing equations are obtained by substituting (2.13) into (2.10) and (2.12). We will extensively employ material descriptions in subsequent sections.

2.5. Domain mapping

The length of the beam outside the guide varies with time, making the reference configuration a varying-length domain. Such problems are best handled by mapping the varying-length domain to a fixed-length domain, see, e.g. Vu-Quoc and Li (1995) or Roy and Chatterjee (2009). Initial length of the beam measured from the origin O of translating frame is represented by L, while $R_0(t) = |\boldsymbol{r}_0(t)|$ represents the length of the beam that remains within the guide. The material point at $S\in[R_0(t),\ L]$ at time t is mapped to $\zeta(S,t)\in[0,\ 1]$ by

$$\zeta(S,t) = 1 + \frac{S-L}{R_1(t)}, \tag{2.14}$$

where $R_1(t) = L - R_0(t)$ is the length of the beam outside the guide. We now define the total derivative $\frac{d(.)}{dt} = \dot{(.)} = \mathring{(.)} + \dot{\zeta}(.)'$ where $(.)' = \frac{\partial(.)}{\partial\zeta}$, $\dot{(.)} = \frac{\partial(.)}{\partial t}|_S$ and $\mathring{(.)} = \frac{\partial(.)}{\partial t}|_\zeta$. From (2.14) we have

$$\dot{\zeta} = (1-\zeta)\frac{\dot{R}_1}{R_1} \quad\text{and}\quad \ddot{\zeta} = (1-\zeta)\frac{\ddot{R}_1}{R_1} - 2(1-\zeta)\left(\frac{\dot{R}_1}{R_1}\right)^2.$$

Fields that were defined in terms of S, which corresponds to the physical domain, are now expressed in terms of ζ which relate to the new, fixed domain. Fields in the new domain will be indicated by a $\tilde{(.)}$. Thus, for example, $\tilde{\boldsymbol{u}}(\zeta,t) = \boldsymbol{u}(S,t)$, $\tilde{\underline{\boldsymbol{\Lambda}}}(\zeta,t) = \underline{\boldsymbol{\Lambda}}(S,t)$, $\tilde{\boldsymbol{w}}(\zeta,t) = \boldsymbol{w}(S,t)$. Utilizing Eqs. (2.14) and the time derivatives presented above, the linear momentum balance (2.10) in the new domain is modified to

$$\tilde{\boldsymbol{n}}'\frac{\partial\zeta}{\partial S} + \tilde{\tilde{\boldsymbol{n}}} = A_\rho\left[\left\{\frac{(1-\zeta)^2\dot{R}_1^2}{R_1^2}\tilde{\boldsymbol{u}}'\right\}' + 2\mathring{\tilde{\boldsymbol{u}}}'\ \frac{(1-\zeta)\dot{R}_1}{R_1} + \tilde{\boldsymbol{u}}'\frac{(1-\zeta)\ddot{R}_1}{R_1} + \mathring{\tilde{\boldsymbol{u}}} - \ddot{\boldsymbol{r}}_0\right]. \tag{2.15}$$

Similarly, angular momentum balance (2.12) becomes

$$\frac{\partial\tilde{\boldsymbol{m}}}{\partial\zeta}\left(\frac{\partial\zeta}{\partial S}\right) + \frac{\partial\tilde{\boldsymbol{\phi}}_0}{\partial\zeta}\left(\frac{\partial\zeta}{\partial S}\right)\times\tilde{\boldsymbol{n}} + \tilde{\tilde{\boldsymbol{m}}} = \underline{\boldsymbol{I}}_\rho\cdot\dot{\tilde{\boldsymbol{w}}} + \tilde{\boldsymbol{w}}\times\left(\underline{\boldsymbol{I}}_\rho\cdot\tilde{\boldsymbol{w}}\right)$$
$$= \tilde{\underline{\boldsymbol{\Lambda}}}\cdot\underline{\boldsymbol{J}}_\rho\cdot\dot{\tilde{\boldsymbol{W}}} + \tilde{\underline{\boldsymbol{\Lambda}}}\cdot\left[\tilde{\boldsymbol{W}}\times\left(\underline{\boldsymbol{J}}_\rho\cdot\tilde{\boldsymbol{W}}\right)\right]. \tag{2.16}$$

The expression for angular velocity $\tilde{\boldsymbol{w}}$ and angular acceleration $\dot{\tilde{\boldsymbol{w}}}$ are evaluated in the new, fixed domain as follows:

$$\text{asym}[\tilde{\boldsymbol{w}}] = \dot{\tilde{\underline{\boldsymbol{\Lambda}}}}\cdot\tilde{\underline{\boldsymbol{\Lambda}}}^T = \left(\mathring{\tilde{\underline{\boldsymbol{\Lambda}}}} + \dot{\zeta}\tilde{\underline{\boldsymbol{\Lambda}}}'\right)\cdot\tilde{\underline{\boldsymbol{\Lambda}}}^T = \text{asym}[\boldsymbol{w}_\zeta] + \dot{\zeta}\,\text{asym}[\boldsymbol{\omega}_\zeta],$$

where $\underline{\boldsymbol{A}} = \text{asym}[\boldsymbol{a}]$ is the skew-symmetric tensor corresponding to the vector $\boldsymbol{a}$ with $A_{ij} = -\epsilon_{ijk}a_k$ in terms of the alternating tensor ϵ_{ijk}, $\boldsymbol{w}_\zeta$ is the axial vector of $\mathring{\tilde{\underline{\boldsymbol{\Lambda}}}}\cdot\tilde{\underline{\boldsymbol{\Lambda}}}^T$ and $\boldsymbol{\omega}_\zeta$ is the axial vector of $\tilde{\underline{\boldsymbol{\Lambda}}}'\cdot\tilde{\underline{\boldsymbol{\Lambda}}}^T$. Thus,

$$\tilde{\boldsymbol{w}} = \boldsymbol{w}_\zeta + \dot{\zeta}\boldsymbol{\omega}_\zeta\,. \tag{2.17}$$

Differentiating $\tilde{\boldsymbol{w}}$ with respect to time yields

$$\dot{\tilde{\boldsymbol{w}}} = \mathring{\tilde{\boldsymbol{w}}} + \dot{\zeta}\tilde{\boldsymbol{w}}' = \mathring{\boldsymbol{w}}_\zeta + \mathring{\dot{\zeta}}\boldsymbol{\omega}_\zeta + \dot{\zeta}\mathring{\boldsymbol{\omega}}_\zeta + \dot{\zeta}(\boldsymbol{w}_\zeta{}' + \dot{\zeta}'\boldsymbol{\omega}_\zeta + \dot{\zeta}\boldsymbol{\omega}_\zeta{}')$$
$$\dot{\tilde{\boldsymbol{w}}} = \mathring{\boldsymbol{w}}_\zeta + \dot{\zeta}^2\boldsymbol{\omega}_\zeta{}' + \ddot{\zeta}\boldsymbol{\omega}_\zeta + \dot{\zeta}(\mathring{\boldsymbol{\omega}}_\zeta + \boldsymbol{w}_\zeta{}'). \tag{2.18}$$

Material counterparts of the above vectors are similarly evaluated as

$$\tilde{\mathbf{W}} = \mathbf{W}_\zeta + \dot{\zeta}\boldsymbol{\kappa}_\zeta \quad\text{and}\quad \dot{\tilde{\mathbf{W}}} = \mathring{\mathbf{W}}_\zeta + \dot{\zeta}^2\boldsymbol{\kappa}_\zeta' + \ddot{\zeta}\boldsymbol{\kappa}_\zeta + \dot{\zeta}\left(\mathring{\boldsymbol{\kappa}}_\zeta + \mathbf{W}_\zeta'\right). \tag{2.19}$$

Similarly, substituting (2.17) and (2.18) into (2.16) yields

$$\tilde{\boldsymbol{m}}'\left(\frac{\partial\zeta}{\partial S}\right) + \tilde{\boldsymbol{\phi}}_0'\left(\frac{\partial\zeta}{\partial S}\right)\times\tilde{\boldsymbol{n}} + \tilde{\tilde{\boldsymbol{m}}}$$
$$= \underline{\boldsymbol{I}}_\rho\cdot\{\mathring{\boldsymbol{w}}_\zeta + \dot{\zeta}^2\boldsymbol{w}_\zeta{}' + \ddot{\zeta}\boldsymbol{\omega}_\zeta + \dot{\zeta}(\mathring{\boldsymbol{\omega}}_\zeta + \boldsymbol{\omega}_\zeta{}')\}$$
$$+ (\boldsymbol{w}_\zeta + \dot{\zeta}\boldsymbol{\omega}_\zeta)\times\left\{\underline{\boldsymbol{I}}_\rho\cdot(\boldsymbol{w}_\zeta + \dot{\zeta}\boldsymbol{\omega}_\zeta)\right\}, \tag{2.20}$$

which, upon using (2.13) and (2.19) can be expressed using variables of the material configuration as:

$$\tilde{\boldsymbol{m}}'\left(\frac{\partial\zeta}{\partial S}\right) + \tilde{\boldsymbol{\phi}}_0'\left(\frac{\partial\zeta}{\partial S}\right)\times\tilde{\boldsymbol{n}} + \tilde{\tilde{\boldsymbol{m}}}$$
$$= \tilde{\underline{\boldsymbol{\Lambda}}}\cdot\underline{\boldsymbol{J}}_\rho\cdot\{\mathring{\boldsymbol{W}}_\zeta + \dot{\zeta}^2\boldsymbol{W}_\zeta{}' + \ddot{\zeta}\boldsymbol{\kappa}_\zeta + \dot{\zeta}(\mathring{\boldsymbol{\kappa}}_\zeta + \boldsymbol{\kappa}_\zeta{}')\}$$
$$+ \tilde{\underline{\boldsymbol{\Lambda}}}\cdot\left[(\boldsymbol{W}_\zeta + \dot{\zeta}\boldsymbol{\kappa}_\zeta)\times\left\{\underline{\boldsymbol{J}}_\rho\cdot(\boldsymbol{W}_\zeta + \dot{\zeta}\boldsymbol{\kappa}_\zeta)\right\}\right], \tag{2.21}$$

Eqs. (2.15) and (2.21) are more convenient for computations, as the underlying computational domain is fixed.

The boundary conditions for the beam in $(\zeta,\ t)$ domain are given by

$$\tilde{\boldsymbol{u}}(\zeta,t) = 0 \quad\text{and}\quad \tilde{\underline{\boldsymbol{\Lambda}}}(\zeta,t) = \underline{\mathbf{1}} \quad\text{at}\quad \zeta = 0,$$
$$\text{and}\quad \tilde{\tilde{\boldsymbol{n}}}(\zeta,t) = 0 \quad\text{and}\quad \tilde{\tilde{\boldsymbol{m}}}(\zeta,t) = 0 \quad\text{at}\quad \zeta = 1, \tag{2.22}$$

which correspond to, respectively, no deformation at the guide's opening and the beam's tip being traction free.

It may be noticed that governing equations are more easily evaluated in terms of $\tilde{\boldsymbol{\phi}}_0$ in comparison to $\tilde{\boldsymbol{u}}$. The utilization of $\tilde{\boldsymbol{u}}$ may appear to be unreasonable, but its importance is revealed in the implementation of the boundary conditions. The boundary condition at $\zeta = 0$ in terms of $\tilde{\boldsymbol{\phi}}_0(\zeta, t)$ would be $\tilde{\boldsymbol{\phi}}_0(\zeta, t) = \boldsymbol{r}_0(t)$, which is not only a time varying condition (making it tougher to apply), but also suggests that the solution depends on the length of the beam inside the guide, which is not true.

3. Finite element formulation

The governing equations are non-linear and cannot be solved through analytical methods. Hence we will utilize the non-linear finite element method (FEM). As this is a transient problem, we will employ Newmark time integration which, in turn, requires finding updates for the primary variables. The configuration of the beam is defined using a linear vector space for the line of centroids and an orthogonal group for the orientation of the cross-section. Because of the latter, it is essential to determine the admissible variations carefully, which is discussed in the next subsection. We then evaluate the weak form and compute its linearization about a given configuration, using the admissible variations. Once the linearized weak form is obtained, we discretize it using Galerkin projections to obtain a system of linear equations for the increments in the beam's deformation.

3.1. Admissible variations

The configuration of a GE beam is defined in terms of the line of centroids $\tilde{\boldsymbol{\phi}}_0(\zeta, t)$ and the orientation of the cross-section, which is followed through the rotation tensor $\underline{\tilde{\boldsymbol{\Lambda}}}(\zeta, t)$.

Consider an arbitrary configuration of the beam given by $\tilde{\boldsymbol{\phi}}(\zeta) := \{\tilde{\boldsymbol{\phi}}_0(\zeta), \underline{\tilde{\boldsymbol{\Lambda}}}(\zeta)\}$. For convenience we do not explicitly show t in the argument in this sub-section. Let $\tilde{\boldsymbol{\phi}}_\varepsilon(\zeta) := \{\tilde{\boldsymbol{\phi}}_{0\varepsilon}(\zeta), \underline{\tilde{\boldsymbol{\Lambda}}}_\varepsilon(\zeta)\}$ be a configuration obtained by a small perturbation of the beam from $\tilde{\boldsymbol{\phi}}(\zeta)$:

$$\tilde{\boldsymbol{\phi}}_{0\varepsilon}(\zeta) = \tilde{\boldsymbol{\phi}}_0(\zeta) + \varepsilon\boldsymbol{\eta}_0(\zeta) \quad \text{and} \quad \underline{\tilde{\boldsymbol{\Lambda}}}_\varepsilon(\zeta) = \underline{\boldsymbol{R}}_\varepsilon(\zeta) \cdot \underline{\tilde{\boldsymbol{\Lambda}}}(\zeta), \tag{3.1}$$

where $\boldsymbol{\eta}_0(\zeta)$ is an arbitrary vector field which, for a small $\varepsilon > 0$, superposes an infinitesimal displacement onto the line of centroids, while $\underline{\boldsymbol{R}}_\varepsilon(\zeta)$ is a superposed infinitesimal rotation. Now, an infinitesimal rotation may be approximated by a *skew-symmetric* tensor $\underline{\boldsymbol{\theta}}$ but, if $\underline{\boldsymbol{R}}_\varepsilon(\zeta)$ is *skew-symmetric*, then $\underline{\tilde{\boldsymbol{\Lambda}}}_\varepsilon(\zeta)$ will not remain orthogonal and, hence, will not represent a configuration of the beam's cross-section.

Employing an orthogonal $\underline{\boldsymbol{R}}_\varepsilon(\zeta)$ will ensure the orthogonality of $\underline{\tilde{\boldsymbol{\Lambda}}}_\varepsilon(\zeta)$, making it an admissible variation. Orthogonal transformation may be obtained by exponentiating a *skew-symmetric* tensor. Therefore we set $\underline{\boldsymbol{R}}_\varepsilon(\zeta) = \exp[\varepsilon\underline{\boldsymbol{\theta}}(\zeta)]$, so that

$$\underline{\tilde{\boldsymbol{\Lambda}}}_\varepsilon(\zeta) = \exp[\varepsilon\underline{\boldsymbol{\theta}}(\zeta)] \cdot \underline{\tilde{\boldsymbol{\Lambda}}}(\zeta). \tag{3.2}$$

Let the axial vector of $\underline{\boldsymbol{\theta}}(\zeta)$ be $\boldsymbol{\vartheta}(\zeta)$. Then, any variation of the form $\boldsymbol{\eta}(\zeta) = \{\boldsymbol{\eta}_0(\zeta), \boldsymbol{\vartheta}(\zeta)\}$, which satisfies the boundary conditions (2.22) will constitute an admissible variation.

The above equations considered variations in the current configuration. Similar variations may also be obtained in the reference configuration by first considering an infinitesimal rotation $\underline{\boldsymbol{R}}^m_\varepsilon(\zeta)$ of the reference configuration followed by the rotation $\underline{\tilde{\boldsymbol{\Lambda}}}(\zeta)$. This process will yield the material counter part $\underline{\boldsymbol{\theta}}^m(\zeta)$ of $\underline{\boldsymbol{\theta}}(\zeta)$:

$$\begin{aligned}\underline{\tilde{\boldsymbol{\Lambda}}}_\varepsilon(\zeta) &= \underline{\boldsymbol{R}}_\varepsilon(\zeta) \cdot \underline{\tilde{\boldsymbol{\Lambda}}}(\zeta) = \underline{\tilde{\boldsymbol{\Lambda}}}(\zeta) \cdot \underline{\boldsymbol{R}}^m_\varepsilon(\zeta) = \exp[\varepsilon\underline{\boldsymbol{\theta}}(\zeta)] \\ &\quad \cdot \underline{\tilde{\boldsymbol{\Lambda}}}(\zeta) = \underline{\tilde{\boldsymbol{\Lambda}}}(\zeta) \cdot \exp[\varepsilon\underline{\boldsymbol{\theta}}^m(\zeta)],\end{aligned} \tag{3.3}$$

where, using the properties of exponential maps, we obtain

$$\underline{\boldsymbol{\theta}}(\zeta) = \underline{\tilde{\boldsymbol{\Lambda}}}(\zeta) \cdot \underline{\boldsymbol{\theta}}^m(\zeta) \cdot \underline{\tilde{\boldsymbol{\Lambda}}}^T(\zeta). \tag{3.4}$$

3.2. The weak form of governing equations

We now derive the weak form of the balance equations. For this we take the inner product of (2.15) and (2.16) with arbitrary admissible variations $\boldsymbol{\eta}_0(\zeta)$ and $\boldsymbol{\vartheta}(\zeta)$, respectively, and add the resultant equations:

$$\begin{aligned}&\int_0^1 \left(\tilde{\boldsymbol{n}}' \frac{\partial\zeta}{\partial S} + \tilde{\tilde{\boldsymbol{n}}}\right) \cdot \boldsymbol{\eta}_0 + \left\{\tilde{\boldsymbol{m}}' \left(\frac{\partial\zeta}{\partial S}\right) + \tilde{\boldsymbol{\phi}}_0' \left(\frac{\partial\zeta}{\partial S}\right) \times \tilde{\boldsymbol{n}} + \tilde{\tilde{\boldsymbol{m}}}\right\} \cdot \boldsymbol{\vartheta}\, d\zeta \\ &= \int_0^1 A_\rho(\ddot{\tilde{\boldsymbol{u}}} - \ddot{\boldsymbol{r}}_0) \cdot \boldsymbol{\eta}_0 + (\underline{\boldsymbol{I}}_\rho \cdot \dot{\tilde{\boldsymbol{w}}} + \tilde{\boldsymbol{w}} \times \underline{\boldsymbol{I}}_\rho \cdot \tilde{\boldsymbol{w}}) \cdot \boldsymbol{\vartheta}\, d\zeta.\end{aligned} \tag{3.5}$$

Let the left hand side of (3.5) be defined as $-G[\tilde{\boldsymbol{\phi}}(\zeta, t), \boldsymbol{\eta}(\zeta)]$, so that (3.5) is rewritten as

$$\begin{aligned}&G[\tilde{\boldsymbol{\phi}}(\zeta, t), \boldsymbol{\eta}(\zeta)] + \int_0^1 A_\rho(\ddot{\tilde{\boldsymbol{u}}} - \ddot{\boldsymbol{r}}_0) \cdot \boldsymbol{\eta}_0 \\ &\quad + (\underline{\boldsymbol{I}}_\rho \cdot \dot{\tilde{\boldsymbol{w}}} + \tilde{\boldsymbol{w}} \times \underline{\boldsymbol{I}}_\rho \cdot \tilde{\boldsymbol{w}}) \cdot \boldsymbol{\vartheta}\, d\zeta = 0.\end{aligned} \tag{3.6}$$

The simplification of $G[\tilde{\boldsymbol{\phi}}(\zeta, t), \boldsymbol{\eta}(\zeta)]$ requires the establishment of strain measures and the constitutive law for the material. To this end, we use the strain measures and the linear-elastic costitutive law presented in Simo (1985), which along with the simplification of $G[\tilde{\boldsymbol{\phi}}(\zeta, t), \boldsymbol{\eta}(\zeta)]$ have been presented in Appendix A. The formulation presented in Appendix A is the same as in Simo and Vu-Quoc (1986) except that the variables have now been mapped to the (ζ, t) domain. We emphasize that the generalized strains, discussed in Simo (1985), captures extension, shear in two planes, torsion, and bending in two directions.

The next step is to expand the acceleration terms of (3.6) in terms of derivatives in the new, fixed domain. The translational and angular acceleration terms will be dealt with separately for convenience. Let the integral associated with translational acceleration terms in (3.6) be called $G_L[\tilde{\boldsymbol{\phi}}(\zeta, t), \boldsymbol{\eta}(\zeta)]$, which is simplified as follows:

$$\begin{aligned}G_L[\tilde{\boldsymbol{\phi}}, \boldsymbol{\eta}] &= \int_0^1 A_\rho(\ddot{\tilde{\boldsymbol{u}}} - \ddot{\boldsymbol{r}}_0) \cdot \boldsymbol{\eta}_0\, d\zeta \\ &= \int_0^1 -A_\rho \left\{\frac{(1-\zeta)^2 \dot{R}_1^2}{R_1^2} \tilde{\boldsymbol{u}}'\right\} \cdot \frac{\partial\boldsymbol{\eta}_0}{\partial\zeta} + A_\rho \left[2\mathring{\tilde{u}}' \frac{(1-\zeta)\dot{R}_1}{R_1}\right. \\ &\quad \left. + \tilde{\boldsymbol{u}}' \frac{(1-\zeta)\ddot{R}_1}{R_1} + \mathring{\tilde{\boldsymbol{u}}} - \ddot{\boldsymbol{r}}_0\right] \cdot \boldsymbol{\eta}_0\, d\zeta,\end{aligned} \tag{3.7}$$

where we have employed the right-hand side of (2.15) to expand $\mathring{\tilde{\boldsymbol{u}}}$, integrated the double derivatives in (2.15) and imposed the boundary condition $\boldsymbol{\eta}_0 = 0$ at $\zeta = 0$.

A similar process is carried out for the angular acceleration integral in (3.6), which we denote by $G_A[\tilde{\boldsymbol{\phi}}(\zeta, t), \boldsymbol{\eta}(\zeta, t)]$. The weak form of these terms are found in the reference configuration, as this simplifies subsequent linearization. The simplification of $G_A[\tilde{\boldsymbol{\phi}}(\zeta, t), \boldsymbol{\eta}(\zeta, t)]$ using the third, fourth and fifth equation of (2.13), and results from (2.19) proceeds as follows:

$$\begin{aligned}G_A[\tilde{\boldsymbol{\phi}}, \boldsymbol{\eta}] &= \int_0^1 (\underline{\boldsymbol{I}}_\rho \cdot \dot{\tilde{\boldsymbol{w}}} + \tilde{\boldsymbol{w}} \times \underline{\boldsymbol{I}}_\rho \cdot \tilde{\boldsymbol{w}}) \cdot \boldsymbol{\vartheta}\, d\zeta \\ &= \int_0^1 \underline{\tilde{\boldsymbol{\Lambda}}} \cdot (\underline{\boldsymbol{J}}_\rho \cdot \dot{\tilde{\boldsymbol{W}}} + \tilde{\boldsymbol{W}} \times \underline{\boldsymbol{J}}_\rho \cdot \tilde{\boldsymbol{W}}) \cdot \boldsymbol{\vartheta}\, d\zeta \\ &= \int_0^1 \underline{\tilde{\boldsymbol{\Lambda}}} \cdot \left[\underline{\boldsymbol{J}}_\rho \cdot \left\{\mathring{\boldsymbol{W}}_\zeta + \dot{\zeta}(\boldsymbol{W}_\zeta' + \mathring{\boldsymbol{\kappa}}_\zeta) + \dot{\zeta}^2 \boldsymbol{\kappa}_\zeta' + \ddot{\zeta}\boldsymbol{\kappa}_\zeta\right\}\right. \\ &\quad \left. + (\boldsymbol{W}_\zeta + \dot{\zeta}\boldsymbol{\kappa}_\zeta) \times \underline{\boldsymbol{J}}_\rho \cdot (\boldsymbol{W}_\zeta + \dot{\zeta}\boldsymbol{\kappa}_\zeta)\right] \cdot \boldsymbol{\vartheta}\, d\zeta.\end{aligned} \tag{3.8}$$

Further progress is made by noting that (see Appendix B):

$$\mathring{\boldsymbol{\kappa}}_\zeta = \boldsymbol{W}_\zeta' + \boldsymbol{\kappa}_\zeta \times \boldsymbol{W}_\zeta. \tag{3.9}$$

Employing expressions for time derivatives of ζ and (3.9) in (3.8) and simplifying gives:

$$\begin{aligned} G_A[\tilde{\boldsymbol{\phi}},\boldsymbol{\eta}] &= \int_0^1 \tilde{\underline{\boldsymbol{\Lambda}}}\cdot\Big[\underline{\boldsymbol{J}}_\rho\cdot\big\{\mathring{\boldsymbol{W}}_\zeta+\dot\zeta(2\boldsymbol{W}'_\zeta+\boldsymbol{\kappa}_\zeta\times\boldsymbol{W}_\zeta)+\dot\zeta^2\boldsymbol{\kappa}'_\zeta+\ddot\zeta\boldsymbol{\kappa}_\zeta\big\}\\ &\quad+(\boldsymbol{W}_\zeta+\dot\zeta\boldsymbol{\kappa}_\zeta)\times\underline{\boldsymbol{J}}_\rho\cdot(\boldsymbol{W}_\zeta+\dot\zeta\boldsymbol{\kappa}_\zeta)\Big]\cdot\boldsymbol{\vartheta}\,d\zeta\\ &= \int_0^1 \tilde{\underline{\boldsymbol{\Lambda}}}\cdot\Big[\underline{\boldsymbol{J}}_\rho\cdot\Big\{\mathring{\boldsymbol{W}}_\zeta+\frac{(1-\zeta)\dot R_1}{R_1}(2\boldsymbol{W}'_\zeta+\boldsymbol{\kappa}_\zeta\times\boldsymbol{W}_\zeta)\\ &\quad+\frac{(1-\zeta)\ddot R_1}{R_1}\boldsymbol{\kappa}_\zeta+\left(\frac{(1-\zeta)^2\dot R_1^2}{R_1^2}\boldsymbol{\kappa}_\zeta\right)'\Big\}\\ &\quad+\left(\boldsymbol{W}_\zeta+\frac{(1-\zeta)\dot R_1}{R_1}\boldsymbol{\kappa}_\zeta\right)\times\underline{\boldsymbol{J}}_\rho\cdot\left(\boldsymbol{W}_\zeta+\frac{(1-\zeta)\dot R_1}{R_1}\boldsymbol{\kappa}_\zeta\right)\Big]\cdot\boldsymbol{\vartheta}\,d\zeta\,. \end{aligned}$$

To proceed further we employ integration by parts to simplify the fourth term in the integral as

$$\begin{aligned} &\int_0^1 \tilde{\underline{\boldsymbol{\Lambda}}}\cdot\underline{\boldsymbol{J}}_\rho\cdot\left(\frac{(1-\zeta)^2\dot R_1^2}{R_1^2}\boldsymbol{\kappa}_\zeta\right)'\cdot\boldsymbol{\vartheta}\,d\zeta\\ &=-\int_0^1\tilde{\underline{\boldsymbol{\Lambda}}}\cdot\left\{\boldsymbol{\kappa}_\zeta\times\underline{\boldsymbol{J}}_\rho\left(\frac{(1-\zeta)^2\dot R_1^2}{R_1^2}\boldsymbol{\kappa}_\zeta\right)\right\}\cdot\boldsymbol{\vartheta}\\ &\quad+\tilde{\underline{\boldsymbol{\Lambda}}}\cdot\underline{\boldsymbol{J}}_\rho\cdot\left(\frac{(1-\zeta)^2\dot R_1^2}{R_1^2}\boldsymbol{\kappa}_\zeta\right)\cdot\boldsymbol{\vartheta}'\,d\zeta\,, \end{aligned}\tag{3.10}$$

where we have imposed the boundary condition $\boldsymbol{\vartheta}=0$ at $\zeta=0$. Substituting (3.10) into the foregoing expression for $G_A[\tilde{\boldsymbol{\phi}},\boldsymbol{\eta}]$ will give its final weak form. The weak form of the system (3.5) may, finally be represented as

$$G_{dyn}[\tilde{\boldsymbol{\phi}},\boldsymbol{\eta}] := G[\tilde{\boldsymbol{\phi}},\boldsymbol{\eta}]+G_L[\tilde{\boldsymbol{\phi}},\tilde{\boldsymbol{\eta}}]+G_A[\tilde{\boldsymbol{\phi}},\tilde{\boldsymbol{\eta}}]=0.\tag{3.11}$$

The governing equations are non-linear, so, to find a solution, it is necessary to linearize the weak form about a proposed configuration and then determine corrections to the proposed configuration. The equation that needs to be solved iteratively to obtain the corrected configuration is given by

$$G_{dyn}[\tilde{\boldsymbol{\phi}}^*,\boldsymbol{\eta}]+\delta G_{dyn}[\tilde{\boldsymbol{\phi}}^*,\boldsymbol{\eta}]=0,\tag{3.12}$$

where $G_{dyn}[\tilde{\boldsymbol{\phi}}^*,\boldsymbol{\eta}]$ is the residual force, which represents the error in the proposed configuration $\tilde{\boldsymbol{\phi}}^*$ and $\delta G_{dyn}[\tilde{\boldsymbol{\phi}}^*,\boldsymbol{\eta}]$ is the linerization about $\tilde{\boldsymbol{\phi}}^*$. To obtain the expression for $\delta G_{dyn}[\tilde{\boldsymbol{\phi}}^*,\boldsymbol{\eta}]$ we need the linearization of time derivatives. This is now discussed.

3.3. Linearization of time derivatives

We will now find expressions for the linearizations of time derivatives, i.e. $\delta\mathring{\tilde{\boldsymbol{u}}}$, $\delta\mathring{\tilde{\boldsymbol{u}}}$, $\delta\boldsymbol{W}_\zeta$, $\delta\mathring{\boldsymbol{W}}_\zeta$. To update fields in time we will rely on the Newmark integration technique.

The linearization of velocity and acceleration is standard (Newmark 1959; Simo and Vu-Quoc 1988; Singh 2018, Section 3.3). For the $\mathrm{n}+1^{\mathrm{st}}$ Newmark time step, the linearizations of velocity and acceleration are, respectively,

$$\begin{aligned} \delta\mathring{\tilde{\mathbf{u}}}^{(\mathrm{j})}(\zeta,\mathrm{t}_{\mathrm{n+1}}) &= \frac{\alpha}{\beta\Delta\mathrm{t}}\Delta\mathbf{u}^{(\mathrm{j})}_{\mathrm{n+1}}\\ \text{and}\qquad \delta\mathring{\tilde{\mathbf{u}}}^{(\mathrm{j})}(\zeta,\mathrm{t}_{\mathrm{n+1}}) &= \frac{1}{\beta\Delta\mathrm{t}^2}\Delta\mathbf{u}^{(\mathrm{j})}_{\mathrm{n+1}}, \end{aligned}\tag{3.13}$$

where $1<\alpha<0$ and $0<\beta<0.5$ are Newmark parameters, the superscript j represents the j^{th} iteration of the Newton-Raphson root finding process during the Newmark time step, $\Delta\boldsymbol{u}^{(j)}_{n+1}$ is the correction in $\tilde{\boldsymbol{u}}^{(j)}_{n+1}$, Δt is the time step between t_n and t_{n+1}, and δ denotes the directional derivative of a field, i.e. for a given vector field $\boldsymbol{F}$,

$$\delta\boldsymbol{F}=\left.\frac{\partial\boldsymbol{F}_\varepsilon}{\partial\varepsilon}\right|_{\varepsilon=0},\tag{3.14}$$

where $\boldsymbol{F}_\varepsilon$ is defined through an equation similar to (3.1). We note that

$$\sum_{j=1}^{j_{max}}\Delta\boldsymbol{u}^{(j)}_{n+1}=\tilde{\boldsymbol{u}}_{n+1}-\tilde{\boldsymbol{u}}_n,$$

where $j_{\max}$ is the number of iterations required to achieve the required accuracy in a Newmark time update. We need to obtain linearizations of angular velocity and angular acceleration. At the same time, rotation rates, e.g. $\tilde{\boldsymbol{w}}_\zeta(\zeta,t)$ and $\mathring{\tilde{\boldsymbol{w}}}_\zeta(\zeta,t)$, are defined in terms of rotation tensors. All these objects at time t_n depend on the orthogonal group $\tilde{\underline{\boldsymbol{\Lambda}}}_n(\zeta):=\tilde{\underline{\boldsymbol{\Lambda}}}(\zeta,t_n)$. It is important to note that rotation tensors, such as $\tilde{\underline{\boldsymbol{\Lambda}}}(\zeta,t)$, do not lie in linear vector spaces. Let the small rotational displacement in the material configuration between times t_n and t_{n+1} be represented by the skew-symmetric tensor $\underline{\boldsymbol{\tau}}^m_n$ (with axial vector $\boldsymbol{\tau}^m_n$). Then we may write

$$\tilde{\underline{\boldsymbol{\Lambda}}}^{(j)}_{n+1}(\zeta)=\tilde{\underline{\boldsymbol{\Lambda}}}_n(\zeta)\cdot\exp[\underline{\boldsymbol{\tau}}^{m(j)}_n]=\exp[\underline{\boldsymbol{\tau}}^{(j)}_n]\cdot\tilde{\underline{\boldsymbol{\Lambda}}}_n(\zeta),\tag{3.15}$$

where $\underline{\boldsymbol{\tau}}^{(j)}_n$ is the spatial counterpart of $\underline{\boldsymbol{\tau}}^{m(j)}_n$, which is the j^{th} iteration of $\underline{\boldsymbol{\tau}}^m_n$ during a Newmark time update step. Simo and Vu-Quoc (1988) then show that

$$\begin{aligned} \delta\boldsymbol{W}^{(j)}_\zeta(\zeta,t_{n+1}) &= \frac{\alpha}{\beta\Delta t}\tilde{\underline{\boldsymbol{\Lambda}}}^{(j)T}_n\cdot\underline{\boldsymbol{T}}(\boldsymbol{\tau}^{(j)}_n)\cdot\Delta\boldsymbol{\theta}^{(j)}_{n+1}\\ \text{and }\delta\mathring{\boldsymbol{W}}^{(j)}_\zeta(\zeta,t_{n+1}) &= \frac{1}{\beta\Delta t^2}\tilde{\underline{\boldsymbol{\Lambda}}}^{(j)T}_n\cdot\underline{\boldsymbol{T}}(\boldsymbol{\tau}^{(j)}_n)\cdot\Delta\boldsymbol{\theta}^{(j)}_{n+1}, \end{aligned}\tag{3.16}$$

where $\Delta\boldsymbol{\theta}^{(j)}_{n+1}$ is such that $\tilde{\underline{\boldsymbol{\Lambda}}}^{(j+1)}_{n+1}=\exp[asym(\Delta\boldsymbol{\theta}^{(j)}_{n+1})]\cdot\tilde{\underline{\boldsymbol{\Lambda}}}^{(j)}_{n+1}$,

$$\underline{\boldsymbol{T}}(\boldsymbol{\tau})=\boldsymbol{e}\otimes\boldsymbol{e}+\frac{|\boldsymbol{\tau}|/2}{\tan(|\boldsymbol{\tau}|/2)}[\mathbf{1}-\boldsymbol{e}\otimes\boldsymbol{e}]-\frac{1}{2}\,\mathrm{asym}(\boldsymbol{\tau})\tag{3.17}$$

and $\boldsymbol{e}=\boldsymbol{\tau}/|\boldsymbol{\tau}|$. From (3.15) and the definition of $\Delta\boldsymbol{\theta}^{(j)}_{n+1}$, we conclude that

$$\exp[\underline{\boldsymbol{\tau}}^{(j+1)}_n]=\exp[asym(\Delta\boldsymbol{\theta}^{(j)}_{n+1})]\cdot\exp[\underline{\boldsymbol{\tau}}^{(j)}_n].\tag{3.18}$$

3.4. Linearization of weak form

We now proceed with the linearization of the weak form (3.11), which can be expressed as

$$\delta G_{dyn}[\tilde{\boldsymbol{\phi}}^*,\boldsymbol{\eta}]=\delta G[\tilde{\boldsymbol{\phi}}^*,\boldsymbol{\eta}]+\delta G_L[\tilde{\boldsymbol{\phi}}^*,\boldsymbol{\eta}]+\delta G_A[\tilde{\boldsymbol{\phi}}^*,\boldsymbol{\eta}].\tag{3.19}$$

Note the linearization is done about a proposed configuration $\tilde{\boldsymbol{\phi}}^*(\zeta,t)=\{\tilde{\boldsymbol{u}}^*(\zeta,t),\tilde{\underline{\boldsymbol{\Lambda}}}^*(\zeta,t)\}$. Let the perturbed configuration be given by $\tilde{\boldsymbol{\phi}}^*_\varepsilon(\zeta,t)=\{\tilde{\boldsymbol{u}}^*_\varepsilon(\zeta,t),\tilde{\underline{\boldsymbol{\Lambda}}}^*_\varepsilon(\zeta,t)\}$, where the perturbation is given as $\Delta\tilde{\boldsymbol{\phi}}^*(\zeta,t)=\{\Delta\tilde{\boldsymbol{u}}^*(\zeta,t),\Delta\tilde{\boldsymbol{\theta}}^*(\zeta,t)\}$. The linearization process will be carried out separately for each term.

Linearization of $G(\tilde{\boldsymbol{\phi}}^*,\boldsymbol{\eta})$ is presented in Appendix A. Unlike the tangent stiffness matrix obtained in non-linear FE formulation of general elasticity, which is symmetric, the linearization of $G(\tilde{\boldsymbol{\phi}}^*,\boldsymbol{\eta})$ yields an unsymmetric tangent stiffness matrix. Here we first present the linearization of $G_L[\tilde{\boldsymbol{\phi}},\boldsymbol{\eta}]$. Utilizing (3.7), we compute

$$\begin{aligned} \delta G_L[\tilde{\boldsymbol{\phi}}^*,\boldsymbol{\eta}] &= \delta\int_0^1 -A_\rho\left\{\frac{(1-\zeta)^2\dot R_1^2}{R_1^2}\tilde{\boldsymbol{u}}'\right\}\cdot\frac{\partial\boldsymbol{\eta}_0}{\partial\zeta}+A_\rho\Big\{2\mathring{\tilde{\boldsymbol{u}}}'\frac{(1-\zeta)\dot R_1}{R_1}\\ &\quad+\tilde{\boldsymbol{u}}'\frac{(1-\zeta)\ddot R_1}{R_1}+\ddot{\tilde{\boldsymbol{u}}}-\ddot{\boldsymbol{r}}_0\Big\}\cdot\boldsymbol{\eta}_0\,d\zeta\\ &= \int_0^1 -A_\rho\left\{\frac{(1-\zeta)^2\dot R_1^2}{R_1^2}(\Delta\tilde{\boldsymbol{u}})'\right\}\cdot\frac{\partial\boldsymbol{\eta}_0}{\partial\zeta}+A_\rho\Big\{2\frac{\alpha}{(\Delta t)\beta}(\Delta\tilde{\boldsymbol{u}})'\frac{(1-\zeta)\dot R_1}{R_1}\\ &\quad+(\Delta\tilde{\boldsymbol{u}})'\frac{(1-\zeta)\ddot R_1}{R_1}+\frac{1}{(\Delta t)^2\beta}\Delta\tilde{\boldsymbol{u}}\Big\}\cdot\boldsymbol{\eta}_0\,d\zeta. \end{aligned}\tag{3.20}$$

The above calculations were carried out using results discussed in the previous section. We may perform the linearization of $G_A[\tilde{\boldsymbol{\phi}}^*, \tilde{\boldsymbol{\eta}}]$ similarly.

However, because the expression for $\delta G_A[\tilde{\boldsymbol{\phi}}^*, \boldsymbol{\eta}]$ is complex, we prefer to write $\delta G_A[\tilde{\boldsymbol{\phi}}^*, \boldsymbol{\eta}] = \delta G_{A1}[\tilde{\boldsymbol{\phi}}^*, \boldsymbol{\eta}] + \delta G_{A2}[\tilde{\boldsymbol{\phi}}^*, \boldsymbol{\eta}] + \delta G_{A\Lambda}[\tilde{\boldsymbol{\phi}}^*, \boldsymbol{\eta}]$, whose computations are given in Appendix C. It may be noted that $\delta G_{A2}[\tilde{\boldsymbol{\phi}}^*, \boldsymbol{\eta}]$ vanishes for planar cases. The above formulation when presented for planar cases matches the formulation presented in Vu-Quoc and Li (1995). Also, because the treatment of finite rotations is performed in the same manner as in Simo and Vu-Quoc (1986), therefore the above formulation when presented for fixed length beams in the physical domain correspond to the expressions in Simo and Vu-Quoc (1986).

In this way we obtain the algebraic equation corresponding to (3.12). This non-linear, algebraic equation will be solved using finite elements and the Newton-Raphson method. This is described next.

3.5. Spatial discretization and configuration updates

In this section we switch from direct notation to matrix notation with all vectors and tensors being evaluated in the fixed frame ($\hat{\boldsymbol{e}}_i$). The notation for matrices and column vectors will be the same as employed for their corresponding tensors and vectors.

We now discuss how we spatially discretize the nonlinear algebraic expression obtained from (3.12) using Galerkin projections and how we update variables in order to implement the Newton-Raphson method. At any time t_{n+1}, the domain $0 \le \zeta \le 1$ is divided into multiple intervals (or elements). Shape functions are utilized to approximate a vector field $\boldsymbol{\alpha}$ over each element as:

$$\boldsymbol{\alpha}(\zeta, t_{n+1}) \simeq \sum_{e=1}^{n_e} N_e(\zeta)\boldsymbol{\alpha}_{e,n+1}, \tag{3.21}$$

where n_e is the number of nodes per element, $N_e(\zeta)$ is the shape function corresponding to the e^{th} node and $\boldsymbol{\alpha}_{e,n+1}$ is the value of the vector field $\boldsymbol{\alpha}$ at the e^{th} node, at time t_{n+1}. The vector field $\boldsymbol{\alpha}$ can be replaced by $\tilde{\boldsymbol{u}}$, $\mathring{\tilde{\boldsymbol{u}}}, \mathring{\mathring{\tilde{\boldsymbol{u}}}}, \tilde{\boldsymbol{W}}$, $\mathring{\tilde{\boldsymbol{W}}}$, $\Delta\tilde{\boldsymbol{u}}$ and $\Delta\tilde{\boldsymbol{\theta}}$ to get their corresponding approximations over the domain. The same shape functions (N_e) are used to approximate the admissible variations.

In contrast, the rotation tensor $\underline{\tilde{\boldsymbol{\Lambda}}}(\zeta, t_{n+1})$ cannot be expressed directly in terms of shape functions. Instead we find the vector $\boldsymbol{\chi}$ such that $\underline{\tilde{\boldsymbol{\Lambda}}} = \exp\{\text{asym}(\boldsymbol{\chi})\}$. Appendix D shows how to compute $\boldsymbol{\chi}$ given $\underline{\tilde{\boldsymbol{\Lambda}}}$. The vector field $\boldsymbol{\chi}$ may be approximated in terms of shape functions as in (3.21). Once $\boldsymbol{\chi}$ is known at the nodes, $\underline{\tilde{\boldsymbol{\Lambda}}}$ over the elements may be found from

$$\underline{\tilde{\boldsymbol{\Lambda}}}(\zeta, t_{n+1}) = \exp\left\{\text{asym}\left(\sum_{e=1}^{n_e} N_e(\zeta)\boldsymbol{\chi}_{e,n+1}\right)\right\}. \tag{3.22}$$

For the problems discussed here we consider two node ($n_e = 2$) linear elements for discretization. After substituting the above approximations into the nonlinear algebraic equation obtained from (3.12), the resulting terms may be represented using matrices. This is demonstrated below using the discretized form over the i^{th} interval (ζ_i, ζ_{i+1}) of the sum of the acceleration terms contained in δG_{A1} and δG_L that are given by, respectively, (C.2) and (3.20):

$$\begin{aligned}
&\frac{1}{\beta(\Delta t)^2}\int_{\zeta_i}^{\zeta_{i+1}} A_\rho \Delta\tilde{\boldsymbol{u}}(\zeta, t_{n+1})\cdot\boldsymbol{\eta}_0 \\
&\quad + \underline{\boldsymbol{\Lambda}}_{n+1}\cdot\underline{\boldsymbol{J}}_\rho\cdot\underline{\boldsymbol{\Lambda}}_n^T\cdot\underline{\boldsymbol{T}}(\boldsymbol{\tau}_n)\cdot\Delta\tilde{\boldsymbol{\theta}}(\zeta, t_{n+1})\cdot\boldsymbol{\vartheta}\, d\zeta \\
&\simeq \frac{1}{\beta(\Delta t)^2}[M_L]\{\Delta\tilde{\boldsymbol{\phi}}\}\cdot\{\boldsymbol{\eta}\}
\end{aligned} \tag{3.23}$$

where

$$(M_L)_{IJ} = \begin{bmatrix}[(m_L)_{IJ}] & [0]_{3\times3} \\ [0]_{3\times3} & [(i_L)_{IJ}]\end{bmatrix},\quad \{\Delta\tilde{\boldsymbol{\phi}}\} = \begin{Bmatrix}\Delta\tilde{\boldsymbol{u}}_e(\zeta_1) \\ \Delta\tilde{\boldsymbol{\theta}}_e(\zeta_1) \\ \Delta\tilde{\boldsymbol{u}}_e(\zeta_2) \\ \Delta\tilde{\boldsymbol{\theta}}_e(\zeta_2)\end{Bmatrix} \text{ and}$$

$$\{\boldsymbol{\eta}\} = \begin{Bmatrix}\boldsymbol{\eta}_e(\zeta_1) \\ \boldsymbol{\vartheta}_e(\zeta_1) \\ \boldsymbol{\eta}_e(\zeta_2) \\ \boldsymbol{\vartheta}_e(\zeta_2)\end{Bmatrix}, \tag{3.24}$$

in which

$$\begin{aligned}
[(m_L)_{IJ}] &= \left\{\int_{\zeta_i}^{\zeta_{i+1}} N_I A_\rho N_J d\zeta\right\}[\underline{1}] \\
\text{and}\quad [(i_L)_{IJ}] &= \int_{\zeta_i}^{\zeta_{i+1}} N_I \underline{\tilde{\boldsymbol{\Lambda}}}_{n+1}\underline{\boldsymbol{J}}_\rho\underline{\tilde{\boldsymbol{\Lambda}}}_n^T\underline{\boldsymbol{T}}(\boldsymbol{\tau}_n)N_J,
\end{aligned} \tag{3.25}$$

where $[\underline{1}]$ is the identity matrix.

To evaluate the integrals over the discretized domain, for example the ones in (3.25), we make use of Gauss quadrature integration. Implementing this requires calculations of variables at points other than the nodes. Except for the rotation tensor ($\underline{\tilde{\boldsymbol{\Lambda}}}$), all other variables can be evaluated over the element by interpolating their values at the nodes using shape functions. The rotation tensor $\underline{\tilde{\boldsymbol{\Lambda}}}$ may be found using the expression (3.22).

We will substitute the approximations (3.21) and (3.22) into the linearized weak form (3.12) to obtain, in each interval (ζ_i, ζ_{i+1}), matrix equations of the kind (3.23). When these matrix equations for all intervals discretizing (0,1) are assembled, we obtain, finally,

$$\{\boldsymbol{\eta}\}.\left[\{\boldsymbol{P}(\tilde{\boldsymbol{\phi}}_{n+1})\} + [K(\underline{\tilde{\boldsymbol{\Lambda}}}_n, \tilde{\boldsymbol{\phi}}_{n+1})]\{\Delta\tilde{\boldsymbol{\phi}}_{n+1}\}\right] = 0, \tag{3.26}$$

where $\{\boldsymbol{P}\}$ is the discretized form of the global force residual vector $G_{dyn}[\tilde{\boldsymbol{\phi}}^*, \boldsymbol{\eta}]$ for the predicted configuration, $[K]$ is the sum of linearized global stiffness and mass matrices found from $\delta G[\tilde{\boldsymbol{\phi}}^*, \boldsymbol{\eta}]$, $\{\Delta\tilde{\boldsymbol{\phi}}_{n+1}\}$ is the incremental displacement and rotation, and $\{\boldsymbol{\eta}\}$ is the vector representing the admissible variations. Because $\boldsymbol{\eta}$ is arbitrary, it is necessary that

$$\{\boldsymbol{P}(\tilde{\boldsymbol{\phi}}_{n+1})\} + [K(\underline{\tilde{\boldsymbol{\Lambda}}}_n, \tilde{\boldsymbol{\phi}}_{n+1})]\{\Delta\tilde{\boldsymbol{\phi}}_{n+1}\} = 0. \tag{3.27}$$

The above is solved for $\Delta\tilde{\boldsymbol{\phi}}_{n+1}$ which, in turn, gives the desired corrected configuration $\tilde{\boldsymbol{\phi}}_{n+1}$ through the use of the Newton-Raphson technique. Once convergence is achieved at t_{n+1} the initial guess for the configuration at the next time step is obtained using the Newmark integration method (Newmark 1959; Singh 2018, Section 3.5).

This concludes the description of our computational algorithm. In the section we apply our algorithm to several problems.

4. Applications

Before proceeding to applications, we note that we have validated our computations by solving several benchmark problems, and these are presented in Singh (2018), Section 4. We will now utilize our computations to investigate the three-dimensional dynamics of a spinning, vibrating, variable-length, flexible beam, whose schematic is show in Fig. 4. We will approach the general situation through a sequence of increasingly complex examples. The various physical properties defined in (A.3) are take to be $EA = 10^6$ N; $GA_1 = 10^5$ N; $GA_2 = 10^5$ N; $GJ = 2\times10^3$ Nm^2; $EI_1 = 10^3$ Nm^2; $EI_2 = 10^3$ Nm^2. We keep $A_\rho = 1$ kg/m and $J_\rho = \text{diag}\{5, 3, 2\}$ kgm^2, where diag{.} indicates a diagonal matrix. The Newmark parameters are kept at $\alpha = 0.5$ and $\beta = 0.25$ unless otherwise specified.

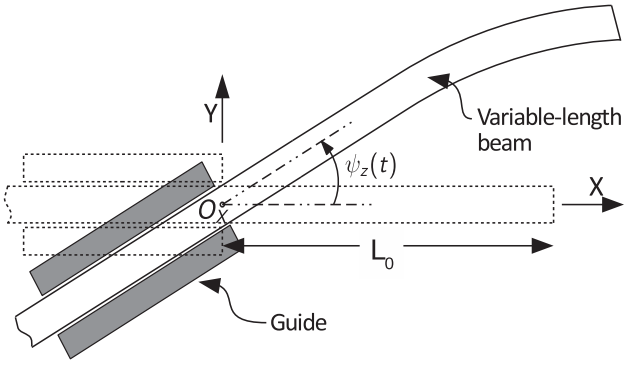

Fig. 4. Schematic of a spinning, vibrating, variable-length, deformable beam. The Z-axis points out of the plane. The X-Y-Z axes are fixed. The angle $\psi_z(t)$ is between the tangent to the centroidal axis at O_X and the fixed X-axis. The guide rotates at a prescribed rate.

4.1. Spinning flexible beam with transverse vibration

We first consider the three-dimensional dynamics of a spinning, and vibrating deformable beam, whose length is taken to be fixed. The in-plane dynamics of such a beam has been considered previously by Simo and Vu-Quoc (1988) and, as validation, we match those results in Singh (2018), Section 4.

We take a 5m beam and divide it into 10 linear elements. We apply an initial transverse load along the Z-axis given by

$$F_z = \begin{cases} \frac{10t}{0.75}\ \text{N} & \text{for } 0 \le t \le 0.75\text{s}, \\ \frac{10(1.5-t)}{0.75}\ \text{N} & \text{for } 0.75\text{s} < t \le 1.5\text{s}. \end{cases} \tag{4.1}$$

After 1.5s the load is removed, but we initiate a rotation at the left hinge about the Z-axis given by

$$\psi_z(t) = \begin{cases} \frac{\pi}{15}\left[\frac{(t-1.5)^2}{2} + \left(\frac{15}{2\pi}\right)^2\left(\cos\left(\frac{2\pi\,(t-1.5)}{15}\right) - 1\right)\right]\text{rad} \\ \qquad\qquad\qquad\qquad \text{for } 1.5\text{s} \le t \le 16.5\text{s} \\ \pi\,(t-1.5) - \frac{15\pi}{2}\ \text{rad} \qquad \text{for } t > 16.5\text{s}. \end{cases} \tag{4.2}$$

This leads to a rotating beam with transverse vibrations. We introduced numerical damping in the Newmark integration process to improve convergence using $\alpha = 0.6$ and $\beta = 0.3025$ and utilizing a time step of $\Delta t = 0.005$s. The values for α and β are calculated using formulae presented in Hilber et al. (1977).

The results are plotted in Fig. 5a which shows all three components of the angular momentum and the external moment about the origin O_X. The match observed between the rate of change of angular momentum and the applied external moment confirms the accuracy of our computations. Fig. 5b displays the transverse vibrations along the Z-axis of the beam's free end with time. Note that both plots in Fig. 5 do not vary much after 16.5s, as beyond that time the imposed rotation rate is constant. We observe in Fig. 5b that, as the rotation rate increases, the transverse deflection of beam reduces. This happens because of centrifugal stiffening.

Fig. 6a and b display the projections of the line of centroids on the XY and XZ-planes, respectively, at different times. While the in-plane (X-Y) deflection is marginal, the out-of-plane deflection is significant.

4.2. Double forced vibration of lengthening beam

We now consider a beam that vibrates in two different planes simultaneously, even as its length changes. To this end we take a 5m long beam divided into 10 equal linear elements. To the tip of

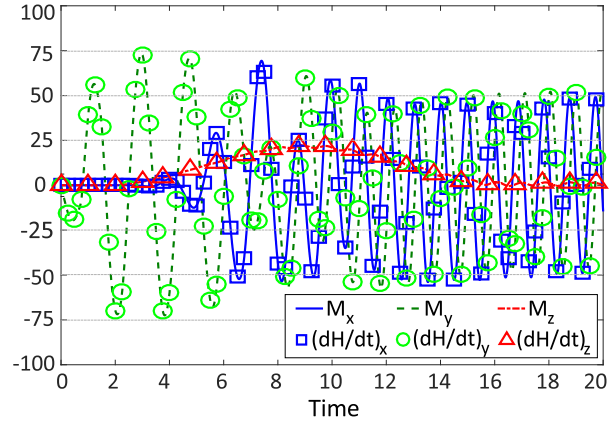

(a) Angular momentum balance

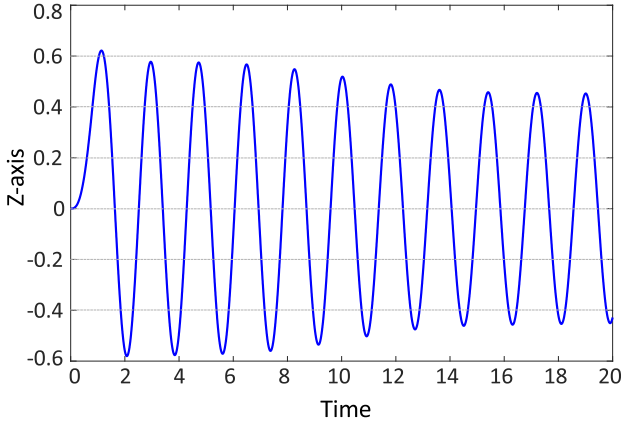

(b) Displacement of the free end.

Fig. 5. (a) Temporal evolution of the rates of change of components of angular momentum $\{(dH/dt)_x, (dH/dt)_y, (dH/dt)_z\}$ and components of external moment $\{M_x, M_y, M_z\}$ about the origin O_X (b) Transverse displacement (along Z-axis) of the beam's free end with time.

the beam we apply forces given by

$$F_z = \begin{cases} \left(\frac{t}{10}\right) \times 100\sin(2\pi t/5)\ \text{N} & \text{for } 0 < t \le 10\text{s}, \\ 100\sin(2\pi t/5)\ \text{N} & \text{for } t > 10\text{s} \end{cases} \tag{4.3}$$

and

$$F_y = \begin{cases} \left(\frac{t-1.25}{10}\right) \times 100\sin(2\pi\,(t-1.25)/5)\ \text{N} \\ \qquad\qquad\qquad\qquad \text{for } 1.25\text{s} < t \le 11.5\text{s}, \\ 100\sin(2\pi\,(t-1.25)/5)\ \text{N} \qquad \text{for } t > 11.5\text{s}. \end{cases} \tag{4.4}$$

Note that the two forces F_z and F_y are separated by a phase difference. At the same time, we start to release the beam at t=0 with a velocity of 0.2 m/s, so that $\dot{R}_1 = 0.2$ m/s. The various physical properties are: $EA = 10^6$ N; $GA_1 = 10^6$ N; $GA_2 = 10^6$ N; $GJ = 10^4$ Nm^2; $EI_1 = 5 \times 10^3$ Nm^2; $EI_2 = 5 \times 10^3$ Nm^2. The values for A_ρ and J_ρ are kept the same as in Section 4.1. The time stepping was kept at $\Delta t = 0.01$s while Newmark coefficients $\alpha = 0.55$ and $\beta = 0.2756$.

Fig. 7 a and b show the projections of the trajectory of the free end on the XZ and YZ planes, respectively. Fig. 7c plots the rate of change of angular momentum about the point O_X along with the applied external moment about that point. The expected match acts as a check of the computation's accuracy. Fig. 8a and b demonstrate the projection of the line of centroids of the beam on the XY and XZ planes respectively, at different times. We now see large deformation in both planes, which is expected given forcing (4.3) and (4.4) in both planes.

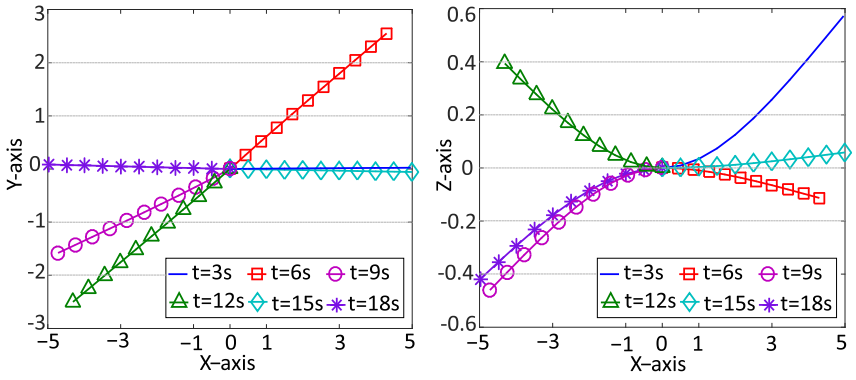

(a) X-Y plane. (b) X-Z plane.

Fig. 6. Projection of the line of centroids of the beam at different instant of time on two different planes.

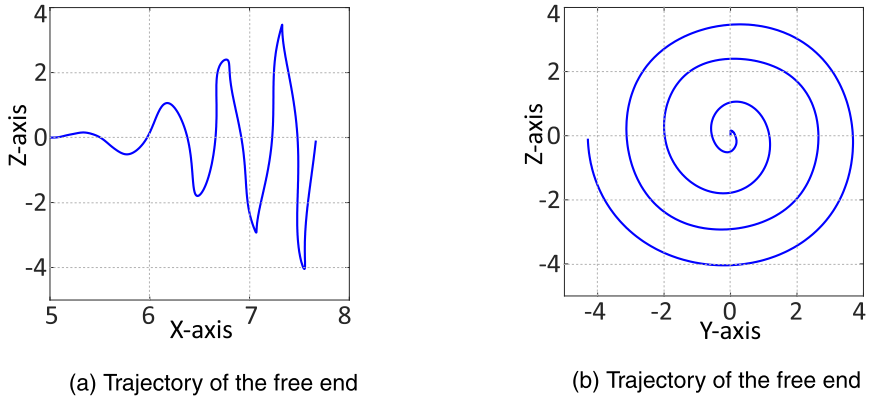

(a) Trajectory of the free end (b) Trajectory of the free end

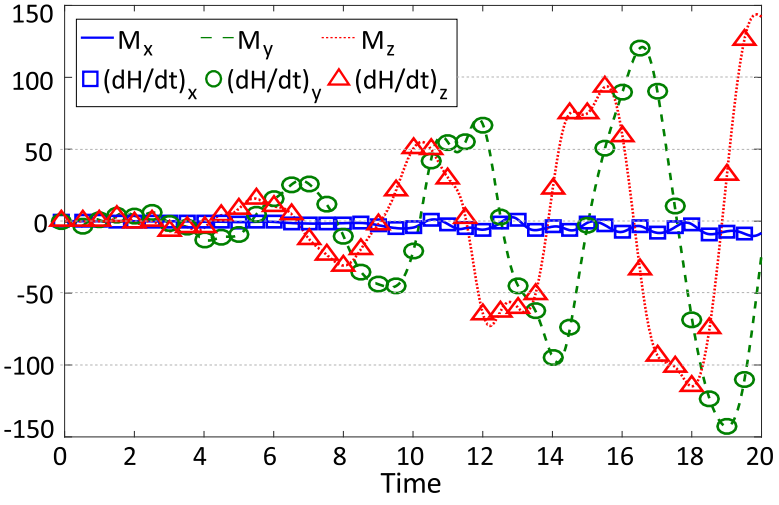

(c) Angular momentum balance

Fig. 7. Trajectory of the beam's free end on (a) X-Z plane and (b) Y-Z plane. (c) Components of the external moment $\{M_x, M_y, M_z\}$ and the components of the rate of change of angular momentum $\{(dH/dT)_x, (dH/dt)_y, (dH/dt)_z\}$ about the origin O_X of fixed frame with time.

4.3. Spinning, lengthening beam with transverse vibration

We now combine simultaneous rotation, out-of-plane vibration and change of length in the same example. To this end, we take a 5m long beam divided into 10 equal linear elements. To the tip of the beam we apply a force given by

$$F_z = \begin{cases} \frac{10(t)}{0.75}\ \text{N} & \text{for } 0 \le t \le 0.75\text{s}, \\ \frac{10(1.5-t)}{0.75}\ \text{N} & \text{for } 0.75\text{s} < t \le 1.5\text{s}. \end{cases} \tag{4.5}$$

After 1.5s the load is removed, but we start to release the beam with a velocity of 0.2 m/s ($= \dot{R}_1$), as well as initiate a rotation at the left hinge about the Z-axis given by

$$\psi_z(t) = \begin{cases} \frac{\pi}{15}\left[\frac{(t-1.5)^2}{2} + \left(\frac{15}{2\pi}\right)^2\left(\cos\left(\frac{2\pi\,(t-1.5)}{15}\right) - 1\right)\right]\text{rad} \\ \qquad\qquad \text{for } 1.5\text{s} \le t \le 16.5\text{s}, \\ \pi\,(t-1.5) - \frac{15\pi}{2}\ \text{rad} \qquad \text{for } t > 16.5\text{s}. \end{cases} \tag{4.6}$$

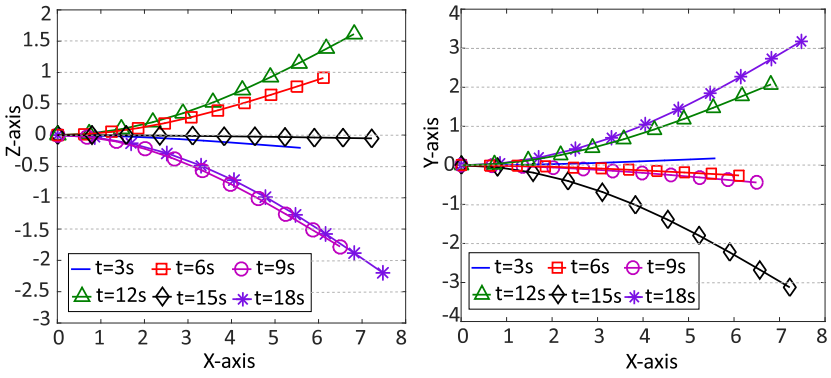

(a) X-Z plane. (b) X-Y plane.

Fig. 8. Projection of the beam's line of centroids at different times on two different planes.

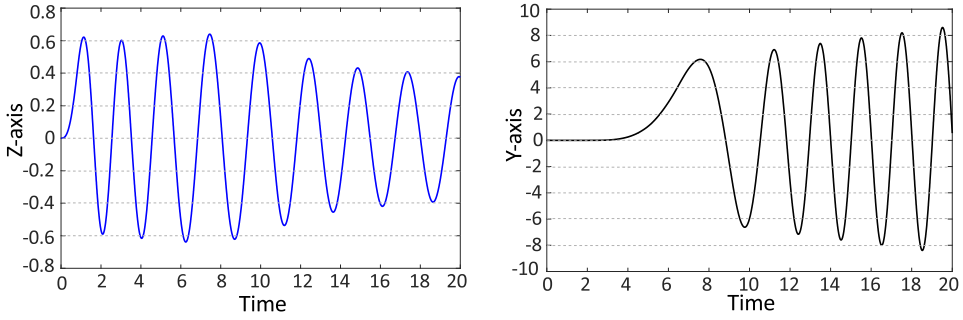

(a) Transverse displacement of free end (b) Displacement of free end

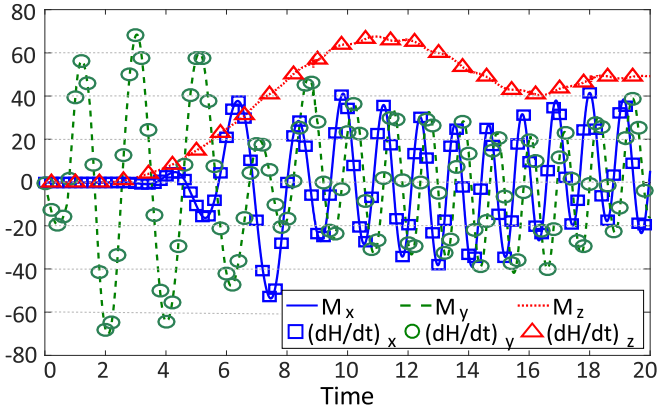

(c) Angular momentum balance.

Fig. 9. Displacement of free end with time along the (a) Z-axis and (b) Y-axis. (c) Temporal variation of the components of external moment $\{M_x, M_y, M_z\}$ and the components of the rate of change of angular momentum $\{(dH/dT)_x, (dH/dt)_y, (dH/dt)_z\}$ about the point O_X.

The time stepping was kept at $\Delta t = 0.005$s while Newmark coefficients $\alpha = 0.6$ and $\beta = 0.3025$.

Fig. 9a and b plots the transverse displacement of free end with time. Note that the amplitude of transverse vibration initially increases due to the beam's lengthening but, as the angular velocity of the beam increases the vibrations start to reduce due to the effects of centrifugal stiffening. Fig. 9c repeats Fig. 7c and plots the rate of change of angular momentum about the point O_X along with the applied external moment about that point. As expected, the two match and this acts as a check of the computation's accuracy. Fig. 10a and b display the projection of the line of centroids on the X-Y and X-Z planes, respectively, at different times. The in-plane deformation, while larger than in Section 4.1, is still smaller than the transverse deformation.

4.4. Transversely vibrating and rotating beam with increasing rate of release

We finally consider an example wherein the rate of change of length of the beam is *not* constant. We take a 5m long beam divided into 10 equal linear elements. To the tip of the beam we apply a force given by

$$F_z = \begin{cases} \frac{20(t)}{0.75}\ \text{N} & \text{for } 0 \le t \le 0.75\text{s} \\ \frac{20(1.5-t)}{0.75}\ \text{N} & \text{for } 0.75\text{s} < t \le 1.5\text{s} \end{cases} \tag{4.7}$$

After 1.5s the load is removed, but we start to release the beam with an acceleration of 0.1 m/s^2 ($= \ddot{R}_1$), as well as initiate a rotation

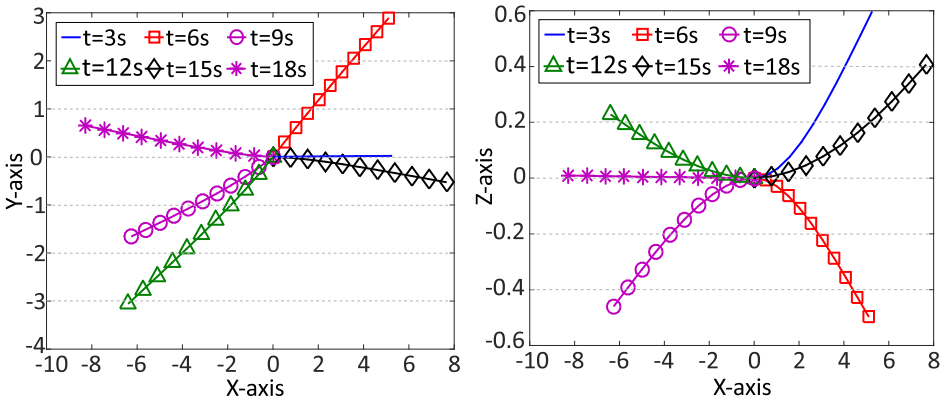

(a) X-Y plane. (b) X-Z plane.

Fig. 10. Projection of the beam's line of centroids at different times on two different planes.

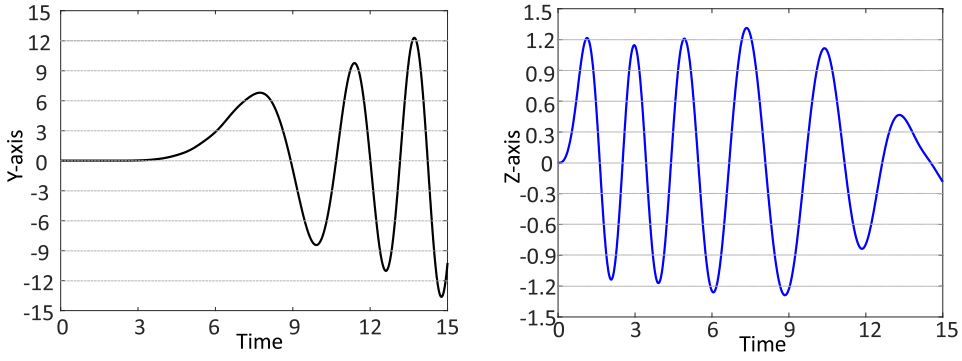

(a) Transverse displacement of free end (b) Transverse displacement of free end

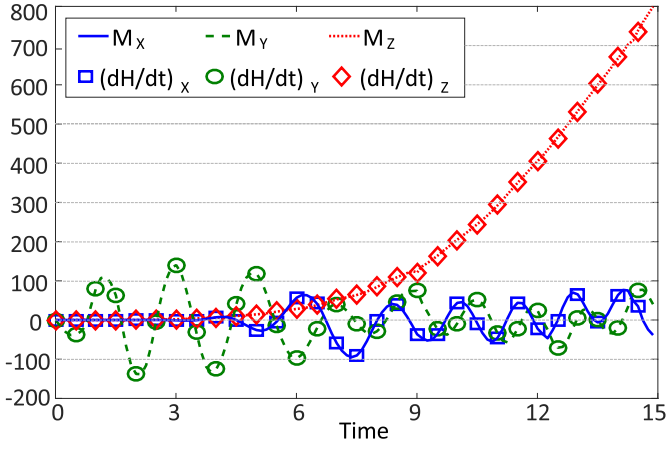

(c) Angular momentum balance.

Fig. 11. Transverse displacement of free end with time along (a) Y-axis and (b) Z-axis. (c) Temporal variation of the components of external moment $\{M_x, M_y, M_z\}$ and the components of the rate of change of angular momentum $\{(dH/dT)_x, (dH/dt)_y, (dH/dt)_z\}$ about the point O_X.

at the left hinge about the Z-axis given by

$$\psi_z(t) = \begin{cases} \frac{\pi}{15}\left[\frac{(t-1.5)^2}{2} + \left(\frac{15}{2\pi}\right)^2\left(\cos\left(\frac{2\pi\,(t-1.5)}{15}\right) - 1\right)\right] \text{rad} \\ \qquad\qquad\qquad\qquad \text{for } 1.5\text{s} \le t \le 16.5\text{s}, \\ \pi\,(t-1.5) - \frac{15\pi}{2} \text{ rad} \qquad \text{for } t > 16.5\text{s}. \end{cases} \tag{4.8}$$

The time stepping was kept at $\Delta t = 0.005$s while the Newmark coefficients $\alpha = 0.6$ and $\beta = 0.3025$.

Fig. 11a and b plot the transverse displacement of the free end with time. In Fig. 11b the amplitude of transverse vibration initially increases due to the beamâs lengthening but, as the angular velocity of the beam increases the vibrations start to reduce due to the effects of centrifugal stiffening. The amplitude of transverse vibration reduces faster in this case compared to the previous example because the length of beam released at any time $t > 4s$ is more in the present case. This in turn increases the centrifugal stiffening which is directly proportional to the beam's length. Fig. 11c plots the rate of change of angular momentum about the point O_X along with the net moment applied about that point. As expected, the

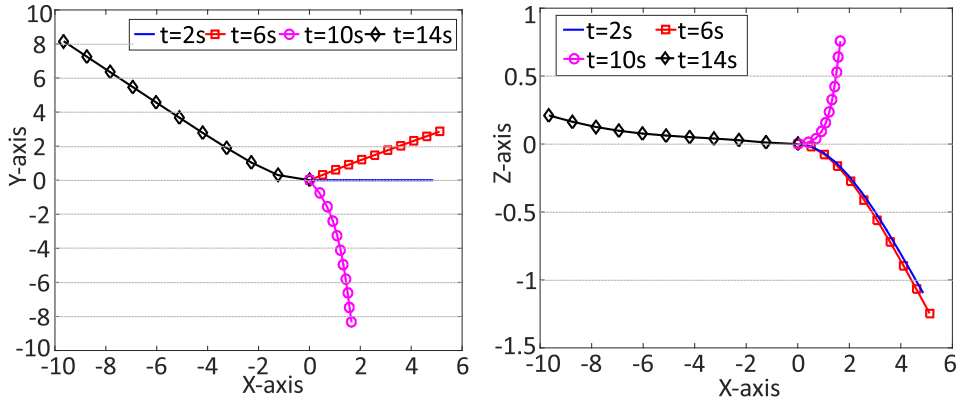

(a) X-Y plane. (b) X-Z plane.

Fig. 12. Projection of the beam's line of centroids at different times on two different planes.

two match. The moment along Z-axis increases rapidly with time because of the increasing rate of release of the cable. Fig. 12a and b display the line of centroids on the XY-plane and XZ-plane, respectively, at different times.

5. Conclusion

In this work we have established the governing equations that determine the three-dimensional dynamics of a variable-length, flexible beam using Geometrically Exact beam theory. Such beams can undergo large deformations and large rotations, with shear deformation being taken into consideration. We incorporated the variable length of the beam by mapping the physical domain on to a fixed domain at each time-step. We then developed an implicit numerical algorithm to solve for the three-dimensional dynamics of such beams. To this end, we found the weak form for the system and subsequently linearizated it before solving the resultant nonlinear algebraic equation by the Newton-Raphson method to obtain the beam's configuration at any given time step. Newmark time integration technique, suitably modified for the orthogonal groups, was employed to perform time updates.

The formulation thus presented matches the results of Simo and Vu-Quoc (1988) obtained for beams of fixed length. Similarly, for planar cases we matched the development of Vu-Quoc and Li (1995). This confirmed the accuracy of our procedure, which we then utilized to investigate the three-dimensional dynamics of spinning, vibrating, variable-length beams through a sequence of increasingly complex examples. We are currently in the process of extending this work to address situations wherein an end mass is attached to the beam. One of the potential application of this work is in the study of release and retraction of aerostats.

Appendix A. Evaluation of $G[\tilde{\boldsymbol{\phi}}, \eta]$ and $\delta G[\tilde{\boldsymbol{\phi}}, \eta]$

Before we proceed to the evaluation of $G[\tilde{\boldsymbol{\phi}}(\zeta,t), \boldsymbol{\eta}(\zeta)]$ and $\delta G[\tilde{\boldsymbol{\phi}}(\zeta,t), \boldsymbol{\eta}(\zeta)]$, it is important to calculate internal force and moment at beam cross-sections. These calculations make use of strain measures defined by

$$\tilde{\boldsymbol{\Gamma}} = \underline{\tilde{\boldsymbol{\Lambda}}}^T \cdot \left[\frac{\partial \tilde{\boldsymbol{u}}}{\partial \zeta}(\zeta,t)\frac{\partial \zeta}{\partial S} + \frac{\partial \boldsymbol{\phi_0}}{\partial S}(S,0) \right] - \hat{\boldsymbol{e}}_3$$

$$\text{and} \quad \tilde{\boldsymbol{\kappa}} = \underline{\tilde{\boldsymbol{\Lambda}}}^T \cdot \tilde{\boldsymbol{\omega}}(\zeta,t) = \underline{\tilde{\boldsymbol{\Lambda}}}^T \cdot \boldsymbol{\omega}_{\zeta}(\zeta,t)\frac{\partial \zeta}{\partial S}, \tag{A.1}$$

where $\tilde{\boldsymbol{\Gamma}}$ and $\tilde{\boldsymbol{\kappa}}$ are strain measures in the material configuration (Simo, 1985). Strain measures in the spatial description are given by $\underline{\tilde{\boldsymbol{\Lambda}}} \cdot \tilde{\boldsymbol{\Gamma}} = \tilde{\boldsymbol{\gamma}}$ and $\tilde{\boldsymbol{\omega}}$, where $\tilde{\boldsymbol{\gamma}}$ may be seen to be the difference in the slope of *line of centroids* and normal to the cross-section, while $\tilde{\boldsymbol{\omega}}$ is the curvature of the rod.

The constitutive law relating the reaction $\tilde{\boldsymbol{R}} := \{\tilde{\boldsymbol{N}}, \tilde{\boldsymbol{M}}\}$ to the strains is taken to be (Simo and Vu-Quoc, 1986; Ibrahimbegović, 1995)

$$\tilde{\boldsymbol{R}} = \begin{Bmatrix} \tilde{\boldsymbol{N}} \\ \tilde{\boldsymbol{M}} \end{Bmatrix} = \underline{\tilde{\boldsymbol{\Lambda}}}^T \cdot \begin{Bmatrix} \tilde{\boldsymbol{n}} \\ \tilde{\boldsymbol{m}} \end{Bmatrix} = \underline{\boldsymbol{C}} \cdot \begin{Bmatrix} \tilde{\boldsymbol{\Gamma}} \\ \tilde{\boldsymbol{\kappa}} \end{Bmatrix}, \tag{A.2}$$

where $\underline{\boldsymbol{C}}$ is the material elasticity tensor (Simo and Vu-Quoc, 1986; Ibrahimbegović, 1995)

$$\underline{\boldsymbol{C}} = diag\big[GA_1, GA_2, EA, EI_1, EI_2, GJ\big]. \tag{A.3}$$

The corresponding stored enery function can be found in Simo and Vu-Quoc (1986). We now proceed to evaluating $G[\tilde{\boldsymbol{\phi}}(\zeta,t), \tilde{\boldsymbol{\eta}}(\zeta)]$ given by

$$G[\tilde{\boldsymbol{\phi}}(\zeta,t), \tilde{\boldsymbol{\eta}}(\zeta)] = -\int_0^1 \left(\tilde{\boldsymbol{n}}' \frac{\partial \zeta}{\partial S} + \tilde{\tilde{\boldsymbol{n}}} \right) \cdot \boldsymbol{\eta}_0 + \left(\tilde{\boldsymbol{m}}' \left(\frac{\partial \zeta}{\partial S} \right) + \tilde{\boldsymbol{\phi}}_0' \left(\frac{\partial \zeta}{\partial S} \right) \times \tilde{\boldsymbol{n}} + \tilde{\tilde{\boldsymbol{m}}} \right) \cdot \boldsymbol{\vartheta} \; d\zeta \, .$$

Using integration by parts we get

$$G[\tilde{\boldsymbol{\phi}}(\zeta,t), \tilde{\boldsymbol{\eta}}(\zeta)] = \left(\frac{d\zeta}{dS} \right) \int_0^1 \left[\tilde{\boldsymbol{n}} \cdot \left\{ \frac{\partial \boldsymbol{\eta}_0}{\partial \zeta} - \left(\boldsymbol{\vartheta} \times \frac{\partial \tilde{\boldsymbol{\phi}}_0}{\partial \zeta} \right) \right\} + \tilde{\boldsymbol{m}} \cdot \frac{\partial \boldsymbol{\vartheta}}{\partial \zeta} \right] d\zeta - \int_0^1 (\tilde{\tilde{\boldsymbol{n}}} \cdot \boldsymbol{\eta}_0 + \tilde{\tilde{\boldsymbol{m}}} \cdot \boldsymbol{\vartheta}) \; d\zeta \, .$$

It is helpful to rewrite the above equation in terms of matrices:

$$G[\tilde{\boldsymbol{\phi}}(\zeta,t), \tilde{\boldsymbol{\eta}}(\zeta)] = \left(\frac{d\zeta}{dS} \right) \int_0^1 (\tilde{\boldsymbol{\Xi}}^T \boldsymbol{\eta}) \cdot (\tilde{\boldsymbol{\Pi}} \tilde{\boldsymbol{R}}) - \left(\frac{dS}{d\zeta} \right) \boldsymbol{\eta} \cdot \tilde{\tilde{\boldsymbol{r}}} \; d\zeta \, , \tag{A.4}$$

where

$$\tilde{\boldsymbol{\Xi}}^T = \begin{bmatrix} \frac{\partial}{\partial \zeta}\underline{\boldsymbol{1}} & \text{asym}\left(\tilde{\boldsymbol{\phi}}_0'\right) \\ \underline{\boldsymbol{0}} & \frac{\partial}{\partial \zeta}\underline{\boldsymbol{1}} \end{bmatrix} \quad , \quad \boldsymbol{\eta} = \begin{bmatrix} \boldsymbol{\eta}_0 \\ \boldsymbol{\vartheta} \end{bmatrix}$$

$$\tilde{\boldsymbol{\Pi}} = \begin{bmatrix} \underline{\tilde{\boldsymbol{\Lambda}}} & \underline{\boldsymbol{0}} \\ \underline{\boldsymbol{0}} & \underline{\tilde{\boldsymbol{\Lambda}}} \end{bmatrix} \quad \text{and} \quad \tilde{\boldsymbol{R}} = \begin{bmatrix} \tilde{\boldsymbol{N}} \\ \tilde{\boldsymbol{M}} \end{bmatrix}.$$

We next compute the linearization of the strain measures:

$$\delta \tilde{\boldsymbol{\Gamma}} = \underline{\tilde{\boldsymbol{\Lambda}}}^T \cdot \left[\frac{\partial (\Delta \tilde{\boldsymbol{u}})}{\partial \zeta} \left(\frac{\partial \zeta}{\partial S} \right) - \Delta \tilde{\boldsymbol{\theta}} \times \left\{ \frac{\partial \tilde{\boldsymbol{u}}}{\partial \zeta} \left(\frac{\partial \zeta}{\partial S} \right) + \frac{\partial \tilde{\boldsymbol{\phi}}_0}{\partial S}(S,0) \right\} \right]$$

$$\text{and} \quad \delta \tilde{\boldsymbol{\kappa}} = \underline{\tilde{\boldsymbol{\Lambda}}}^T \cdot \frac{\partial (\Delta \tilde{\boldsymbol{\theta}})}{\partial \zeta} \left(\frac{\partial \zeta}{\partial S} \right). \tag{A.5}$$

The following simplifictaion of $\delta G[\tilde{\boldsymbol{\phi}}(\zeta,t),\boldsymbol{\eta}(\zeta)]$ may be found in Simo and Vu-Quoc (1986):

$$\begin{aligned}\delta G[\tilde{\boldsymbol{\phi}},\boldsymbol{\eta}] &= \left.\frac{dG[\tilde{\boldsymbol{\phi}}_\varepsilon,\boldsymbol{\eta}]}{d\varepsilon}\right|_{\varepsilon=0} = \left(\frac{d\zeta}{dS}\right)\int_0^1 \left.\frac{d}{d\varepsilon}\right|_{\varepsilon=0} \\ &\quad \times (\boldsymbol{\Xi}_\varepsilon^T\boldsymbol{\eta})\cdot(\boldsymbol{\Pi}_\varepsilon\boldsymbol{R}_\varepsilon) - \left(\frac{dS}{d\zeta}\right)\boldsymbol{\eta}\cdot\tilde{\boldsymbol{r}}\,d\zeta \\ &= \left(\frac{d\zeta}{dS}\right)\int_0^1 \left.\frac{d}{d\varepsilon}\right|_{\varepsilon=0} (\boldsymbol{\Xi}_\varepsilon^T\boldsymbol{\eta})\cdot(\boldsymbol{\Pi}_\varepsilon\boldsymbol{R}_\varepsilon)d\zeta \\ &= \left(\frac{d\zeta}{dS}\right)\int_0^1 \left(\frac{d\boldsymbol{\Xi}_\varepsilon^T}{d\varepsilon}\boldsymbol{\eta}\cdot(\boldsymbol{\Pi}_\varepsilon\boldsymbol{R}_\varepsilon) + (\boldsymbol{\Xi}_\varepsilon^T\boldsymbol{\eta})\cdot\frac{d\boldsymbol{\Pi}_\varepsilon}{d\varepsilon}\boldsymbol{R}_\varepsilon\right. \\ &\quad \left. + (\boldsymbol{\Xi}_\varepsilon^T\boldsymbol{\eta})\cdot\boldsymbol{\Pi}_\varepsilon\frac{d\boldsymbol{R}_\varepsilon}{d\varepsilon}\right)\Bigg|_{\varepsilon=0} d\zeta. \end{aligned} \tag{A.6}$$

The evaluations for the three terms is now carried out separately for convenience. Evaluating the first and second term yields:

$$\left.\frac{d\boldsymbol{\Xi}_\varepsilon^T}{d\varepsilon}\boldsymbol{\eta}\cdot(\boldsymbol{\Pi}_\varepsilon\boldsymbol{R}_\varepsilon)\right|_{\varepsilon=0} = \begin{bmatrix}\underline{\mathbf{0}} & \operatorname{asym}\left(\Delta\tilde{\boldsymbol{u}}'\right)\\ \underline{\mathbf{0}} & \underline{\mathbf{0}}\end{bmatrix}\boldsymbol{\eta}\cdot(\boldsymbol{\Pi}\boldsymbol{R}) \tag{A.7}$$

and

$$\left.\left(\boldsymbol{\Xi}_\varepsilon^T\boldsymbol{\eta}\right)\cdot\frac{d\boldsymbol{\Pi}_\varepsilon}{d\varepsilon}\boldsymbol{R}_\varepsilon\right|_{\varepsilon=0} = (\boldsymbol{\Xi}^T\boldsymbol{\eta})\cdot\begin{bmatrix}\operatorname{asym}\left(\Delta\tilde{\boldsymbol{\theta}}\right) & \underline{\mathbf{0}}\\ \underline{\mathbf{0}} & \operatorname{asym}\left(\Delta\tilde{\boldsymbol{\theta}}\right)\end{bmatrix}\boldsymbol{\Pi}\boldsymbol{R}. \tag{A.8}$$

To evaluate the third term in (A.6) we make use of the constitutive relations (A.2). Applying (A.1), (A.2) and (A.5) to solve the third term gives:

$$\begin{aligned}(\boldsymbol{\Xi}_\varepsilon^T\boldsymbol{\eta})\cdot\boldsymbol{\Pi}_\varepsilon\left.\frac{d\boldsymbol{R}_\varepsilon}{d\varepsilon}\right|_{\varepsilon=0} &= (\boldsymbol{\Xi}_\varepsilon^T\boldsymbol{\eta})\cdot\boldsymbol{\Pi}C\begin{bmatrix}\delta\tilde{\boldsymbol{\Gamma}}\\ \delta\tilde{\boldsymbol{\kappa}}\end{bmatrix} \\ &= \left(\frac{d\zeta}{dS}\right)\boldsymbol{\Xi}^T\boldsymbol{\eta}\cdot\boldsymbol{\Pi}C\boldsymbol{\Pi}^T\boldsymbol{\Xi}^T\Delta\tilde{\boldsymbol{\phi}}. \end{aligned} \tag{A.9}$$

Adding (A.7)-(A.9) will give $\delta G[\tilde{\boldsymbol{\phi}},\boldsymbol{\eta}]$ which on after rearrangement can be expressed as:

$$\begin{aligned}\delta G[\tilde{\boldsymbol{\phi}},\tilde{\boldsymbol{\eta}}] &= \left(\frac{d\zeta}{dS}\right)\int_0^1 (\Psi^T\tilde{\boldsymbol{\eta}})\cdot(B\Psi^T\Delta\tilde{\boldsymbol{\phi}}) \\ &\quad + \left(\frac{d\zeta}{dS}\right)\boldsymbol{\Xi}^T\boldsymbol{\eta}\cdot\boldsymbol{\Pi}C\boldsymbol{\Pi}^T\boldsymbol{\Xi}^T\Delta\tilde{\boldsymbol{\phi}}\,d\zeta \end{aligned} \tag{A.10}$$

where

$$\Psi^T = \begin{bmatrix}\frac{d}{d\zeta}\underline{\mathbf{1}} & \underline{\mathbf{0}}\\ \underline{\mathbf{0}} & \frac{d}{d\zeta}\underline{\mathbf{1}}\\ \underline{\mathbf{0}} & \underline{\mathbf{1}}\end{bmatrix} \quad\text{and}\quad B = \begin{bmatrix}\underline{\mathbf{0}} & \underline{\mathbf{0}} & \operatorname{asym}(-\boldsymbol{n})\\ \underline{\mathbf{0}} & \underline{\mathbf{0}} & \operatorname{asym}(\boldsymbol{m})\\ \operatorname{asym}(\boldsymbol{n}) & \underline{\mathbf{0}} & (\boldsymbol{n}\otimes\boldsymbol{\phi}_0') - (\boldsymbol{n}.\boldsymbol{\phi}_0')\underline{\mathbf{1}}\end{bmatrix}. \tag{A.11}$$

Hence, the linearization of $\delta G[\tilde{\boldsymbol{\phi}},\boldsymbol{\eta}]$ can be expressed using two terms. The first term in (A.10) is called geometric stiffness matrix while the second represents material stiffness matrix.

Appendix B. Derivation of $\mathring{\boldsymbol{\kappa}}_\zeta$

To prove (3.10) we make use the basic definitions of $\boldsymbol{\kappa}_\zeta$,$\boldsymbol{W}_\zeta$, properties of skew-symmetric tensors and expansion for vector triple products. The time derivative of $\mathring{\boldsymbol{\kappa}}_\zeta$ can be expressed as follows:

$$\begin{aligned}\operatorname{asym}\left(\mathring{\boldsymbol{\kappa}}_\zeta\right) &= (\mathring{\underline{\boldsymbol{\Lambda}}}^T\cdot\underline{\boldsymbol{\Lambda}}') = \mathring{\underline{\boldsymbol{\Lambda}}}^T\cdot\underline{\boldsymbol{\Lambda}}' \\ &\quad + \underline{\boldsymbol{\Lambda}}^T\cdot(\mathring{\underline{\boldsymbol{\Lambda}}}') = \mathring{\underline{\boldsymbol{\Lambda}}}^T\cdot\underline{\boldsymbol{\Lambda}}' + \operatorname{asym}\left(\boldsymbol{W}_\zeta'\right) - (\underline{\boldsymbol{\Lambda}}')^T\cdot\mathring{\underline{\boldsymbol{\Lambda}}} \\ &= \operatorname{asym}\left(\boldsymbol{W}_\zeta'\right) + \mathring{\underline{\boldsymbol{\Lambda}}}^T\cdot\underline{\boldsymbol{\Lambda}}' - \left(\mathring{\underline{\boldsymbol{\Lambda}}}^T\cdot\underline{\boldsymbol{\Lambda}}'\right)^T \\ &= \operatorname{asym}\left(\boldsymbol{W}_\zeta'\right) + \operatorname{asym}\left(\boldsymbol{W}_\zeta\right)^T\operatorname{asym}\left(\boldsymbol{\kappa}_\zeta\right) \\ &\quad - \operatorname{asym}\left(\boldsymbol{\kappa}_\zeta\right)^T\operatorname{asym}\left(\boldsymbol{W}_\zeta\right) \\ &= \operatorname{asym}\left(\boldsymbol{W}_\zeta'\right) + \operatorname{asym}\left(\boldsymbol{\kappa}_\zeta\right)\operatorname{asym}\left(\boldsymbol{W}_\zeta\right) \\ &\quad - \operatorname{asym}\left(\boldsymbol{W}_\zeta\right)\operatorname{asym}\left(\boldsymbol{\kappa}_\zeta\right). \end{aligned} \tag{B.1}$$

Now we attempt to find the axial vector of tensors of the above equation:

$$\mathring{\boldsymbol{\kappa}}_\zeta = \boldsymbol{W}_\zeta' + axial\left(\operatorname{asym}\left(\boldsymbol{\kappa}_\zeta\right)\operatorname{asym}\left(\boldsymbol{W}_\zeta\right) - \operatorname{asym}\left(\boldsymbol{W}_\zeta\right)\operatorname{asym}\left(\boldsymbol{\kappa}_\zeta\right)\right).$$

To determine the axial vector on the right side of the above equation we operate it on a random vector $\boldsymbol{h}$:

$$\begin{aligned}&\left[\operatorname{asym}\left(\boldsymbol{\kappa}_\zeta\right)\operatorname{asym}\left(\boldsymbol{W}_\zeta\right) - \operatorname{asym}\left(\boldsymbol{W}_\zeta\right)\operatorname{asym}\left(\boldsymbol{\kappa}_\zeta\right)\right]\cdot\boldsymbol{h} \\ &\quad = \boldsymbol{\kappa}_\zeta\times(\boldsymbol{W}_\zeta\times\boldsymbol{h}) - \boldsymbol{W}_\zeta\times(\boldsymbol{\kappa}_\zeta\times\boldsymbol{h}) = \left(\boldsymbol{\kappa}_\zeta\times\boldsymbol{W}_\zeta\right)\times\boldsymbol{h}. \end{aligned} \tag{B.2}$$

Thus, $axial\left(\operatorname{asym}\left(\boldsymbol{\kappa}_\zeta\right)\operatorname{asym}\left(\boldsymbol{W}_\zeta\right) - \operatorname{asym}\left(\boldsymbol{W}_\zeta\right)\operatorname{asym}\left(\boldsymbol{\kappa}_\zeta\right)\right) = \left(\boldsymbol{\kappa}_\zeta\times\boldsymbol{W}_\zeta\right)$.

Substituting the above result into (B.1) we obtain:

$$\mathring{\boldsymbol{\kappa}}_\zeta = \boldsymbol{W}_\zeta' + \boldsymbol{\kappa}_\zeta\times\boldsymbol{W}_\zeta. \tag{B.3}$$

Appendix C. Evaluation of $\delta G_{A1}[\tilde{\boldsymbol{\phi}},\tilde{\boldsymbol{\eta}}]$, $\delta G_{A2}[\tilde{\boldsymbol{\phi}},\tilde{\boldsymbol{\eta}}]$ and $\delta G_{A\Lambda}[\tilde{\boldsymbol{\phi}},\tilde{\boldsymbol{\eta}}]$

We have

$$\begin{aligned}\delta G_{A1}[\tilde{\boldsymbol{\phi}},\tilde{\boldsymbol{\eta}}] &= \int_0^1 \underline{\tilde{\boldsymbol{\Lambda}}}\cdot\delta\left[\underline{\boldsymbol{J}}_\rho\cdot\left\{\dot{\boldsymbol{W}}_\zeta + \frac{(1-\zeta)\dot{R}_1}{R_1}(2\,\boldsymbol{W}_\zeta' + \boldsymbol{\kappa}_\zeta\times\boldsymbol{W}_\zeta)\right.\right. \\ &\quad \left.\left. + \frac{(1-\zeta)\ddot{R}_1}{R_1}\boldsymbol{\kappa}_\zeta\right\} - \frac{(1-\zeta)^2\dot{R}_1^2}{R_1^2}\left(\boldsymbol{\kappa}_\zeta\times\underline{\boldsymbol{J}}_\rho\cdot\boldsymbol{\kappa}_\zeta\right)\right]\cdot\boldsymbol{\vartheta}\,d\zeta \\ &\quad - \left(\frac{dS}{d\zeta}\right)\int_0^1 \underline{\tilde{\boldsymbol{\Lambda}}}\cdot\delta\left[\underline{\boldsymbol{J}}_\rho\cdot\left(\frac{(1-\zeta)^2\dot{R}_1^2}{R_1^2}\boldsymbol{\kappa}_\zeta\right)\right]\cdot\boldsymbol{\vartheta}'\,d\zeta. \end{aligned} \tag{C.1}$$

Evaluating each term form the above equation separately gives

$$\begin{aligned}&\int_0^1 \underline{\tilde{\boldsymbol{\Lambda}}}\cdot\underline{\boldsymbol{J}}_\rho\cdot\delta\dot{\boldsymbol{W}}_\zeta\cdot\boldsymbol{\vartheta}\,d\zeta = \frac{1}{\beta\Delta t^2}\int_0^1 \underline{\tilde{\boldsymbol{\Lambda}}}_{n+1}\cdot\underline{\boldsymbol{J}}_\rho\cdot\underline{\tilde{\boldsymbol{\Lambda}}}_n^T\cdot\underline{\boldsymbol{T}}\cdot(\boldsymbol{\tau}_n)\Delta\boldsymbol{\theta}_{n+1}\cdot\boldsymbol{\vartheta}\,d\zeta, \\ &2\int_0^1 \underline{\tilde{\boldsymbol{\Lambda}}}\cdot\underline{\boldsymbol{J}}_\rho\cdot\frac{(1-\zeta)\dot{R}_1}{R_1}(\delta\boldsymbol{W}_\zeta')\cdot\boldsymbol{\vartheta}\,d\zeta = \frac{2\alpha}{\beta\Delta t}\int_0^1 \frac{(1-\zeta)\dot{R}_1}{R_1}\underline{\tilde{\boldsymbol{\Lambda}}}_{n+1}\cdot\underline{\boldsymbol{J}}_\rho \\ &\quad\cdot\left((\underline{\tilde{\boldsymbol{\Lambda}}}_n')^T\cdot\underline{\boldsymbol{T}}(\boldsymbol{\tau}_n)\cdot\Delta\boldsymbol{\theta}_{n+1} + \underline{\tilde{\boldsymbol{\Lambda}}}_n^T\cdot\underline{\boldsymbol{T}}'(\boldsymbol{\tau}_n)\cdot\Delta\boldsymbol{\theta}_{n+1} + \underline{\tilde{\boldsymbol{\Lambda}}}_n^T\cdot\underline{\boldsymbol{T}}(\boldsymbol{\tau}_n)\cdot\Delta\boldsymbol{\theta}_{n+1}'\right) \\ &\quad\cdot\boldsymbol{\vartheta}\,d\zeta, \\ &\int_0^1 \underline{\tilde{\boldsymbol{\Lambda}}}\cdot\underline{\boldsymbol{J}}_\rho\cdot\frac{(1-\zeta)\dot{R}_1}{R_1}\delta(\boldsymbol{\kappa}_\zeta\times\boldsymbol{W}_\zeta)\cdot\boldsymbol{\vartheta}\,d\zeta = \int_0^1 \frac{(1-\zeta)\dot{R}_1}{R_1}\underline{\tilde{\boldsymbol{\Lambda}}}_{n+1}\cdot\underline{\boldsymbol{J}}_\rho \\ &\quad\cdot\left(\frac{\alpha}{\beta\Delta t}\operatorname{asym}[\boldsymbol{\kappa}_\zeta]\cdot\underline{\tilde{\boldsymbol{\Lambda}}}_n^T\cdot\underline{\boldsymbol{T}}(\boldsymbol{\tau}_n)\cdot\Delta\boldsymbol{\theta}_{n+1} - \operatorname{asym}[\boldsymbol{W}_\zeta]\cdot\underline{\tilde{\boldsymbol{\Lambda}}}_{n+1}^T\cdot\Delta\boldsymbol{\theta}_{n+1}'\right) \\ &\quad\cdot\boldsymbol{\vartheta}\,d\zeta, \\ &\int_0^1 \underline{\tilde{\boldsymbol{\Lambda}}}\cdot\underline{\boldsymbol{J}}_\rho\cdot\frac{(1-\zeta)\ddot{R}_1}{R_1}\delta\boldsymbol{\kappa}_\zeta\cdot\boldsymbol{\vartheta}d\zeta \\ &\quad = \int_0^1 \frac{(1-\zeta)\ddot{R}_1}{R_1}\underline{\tilde{\boldsymbol{\Lambda}}}_{n+1}\cdot\underline{\boldsymbol{J}}_\rho\cdot\underline{\tilde{\boldsymbol{\Lambda}}}_{n+1}^T\cdot\Delta\boldsymbol{\theta}_{n+1}'\cdot\boldsymbol{\vartheta}\,d\zeta, \\ &\int_0^1 \underline{\tilde{\boldsymbol{\Lambda}}}\cdot\delta\left[\underline{\boldsymbol{J}}_\rho\cdot\left(\frac{(1-\zeta)^2\dot{R}_1^2}{R_1^2}\boldsymbol{\kappa}_\zeta\right)\right]\cdot\boldsymbol{\vartheta}'\,d\zeta \\ &\quad = \int_0^1 \frac{(1-\zeta)^2\dot{R}_1^2}{R_1^2}\underline{\tilde{\boldsymbol{\Lambda}}}_{n+1}\cdot\underline{\boldsymbol{J}}_\rho\cdot\underline{\tilde{\boldsymbol{\Lambda}}}_{n+1}^T\cdot\Delta\boldsymbol{\theta}_{n+1}'\cdot\boldsymbol{\vartheta}'\,d\zeta, \\ &\int_0^1 \underline{\tilde{\boldsymbol{\Lambda}}}\cdot\delta\left\{\boldsymbol{\kappa}_\zeta\times\underline{\boldsymbol{J}}_\rho\cdot\boldsymbol{\kappa}_\zeta\right\}\cdot\boldsymbol{\vartheta}\,d\zeta = \int_0^1 \underline{\tilde{\boldsymbol{\Lambda}}}_{n+1}\cdot\left\{\operatorname{asym}[\boldsymbol{\kappa}_\zeta]\cdot\underline{\boldsymbol{J}}_\rho - \operatorname{asym}[\underline{\boldsymbol{J}}_\rho\cdot\boldsymbol{\kappa}_\zeta]\right\} \\ &\quad\cdot\underline{\tilde{\boldsymbol{\Lambda}}}_{n+1}^T\cdot\Delta\boldsymbol{\theta}_{n+1}'\cdot\boldsymbol{\vartheta}d\zeta. \end{aligned} \tag{C.2}$$

The linearization of G_{A2} is expressed as

$$\begin{aligned}\delta G_{A2}[\tilde{\boldsymbol{\phi}},\tilde{\boldsymbol{\eta}}] &= \int_0^1 \tilde{\underline{\boldsymbol{\Lambda}}}\cdot\delta\left[\left(\boldsymbol{W}_\zeta+\frac{(1-\zeta)\dot{R}_1}{R_1}\boldsymbol{\kappa}_\zeta\right)\right.\\ &\quad\left.\times\underline{\boldsymbol{J}}_\rho\cdot\left(\boldsymbol{W}_\zeta+\frac{(1-\zeta)\dot{R}_1}{R_1}\boldsymbol{\kappa}_\zeta\right)\right]\cdot\boldsymbol{\vartheta}\,d\zeta\\ &= \int_0^1 \tilde{\underline{\boldsymbol{\Lambda}}}\cdot\delta(\tilde{\boldsymbol{W}}\times\underline{\boldsymbol{J}}_\rho\cdot\tilde{\boldsymbol{W}})\cdot\boldsymbol{\vartheta}\;d\zeta\\ &= \int_0^1 \tilde{\underline{\boldsymbol{\Lambda}}}_{n+1}\cdot\left(\text{asym}[\tilde{\boldsymbol{W}}]\cdot\underline{\boldsymbol{J}}_\rho-\text{asym}[\underline{\boldsymbol{J}}_\rho\cdot\tilde{\boldsymbol{W}}]\right)\\ &\quad\cdot\left(\frac{\alpha}{\beta\Delta t}\underline{\boldsymbol{\Lambda}}_n^T\cdot\underline{\boldsymbol{T}}(\boldsymbol{\tau}_n)\cdot\Delta\boldsymbol{\theta}_{n+1}\right.\\ &\quad\left.+\frac{(1-\zeta)\dot{R}_1}{R_1}\tilde{\underline{\boldsymbol{\Lambda}}}_{n+1}^T\cdot\Delta\boldsymbol{\theta}'_{n+1}\right)\cdot\boldsymbol{\vartheta}\;d\zeta\,. \end{aligned}\tag{C.3}$$

The linearization of $G_{A\Lambda}$ is evaluated as

$$\begin{aligned}\delta G_{A\Lambda}[\tilde{\boldsymbol{\phi}},\tilde{\boldsymbol{\eta}}] &= \int_0^1(\delta\tilde{\underline{\boldsymbol{\Lambda}}})\cdot\left[\underline{\boldsymbol{J}}_\rho\cdot\left\{\mathring{\boldsymbol{W}}_\zeta+\frac{(1-\zeta)\dot{R}_1}{R_1}(2\,\boldsymbol{W}'_\zeta+\boldsymbol{\kappa}_\zeta\times\boldsymbol{W}_\zeta)\right.\right.\\ &\quad\left.\left.+\frac{(1-\zeta)\ddot{R}_1}{R_1}\boldsymbol{\kappa}_\zeta\right\}-\frac{(1-\zeta)^2\dot{R}_1^2}{R_1^2}\left(\boldsymbol{\kappa}_\zeta\times\underline{\boldsymbol{J}}_\rho\cdot\boldsymbol{\kappa}_\zeta\right)\right]\cdot\boldsymbol{\vartheta}\;d\zeta\\ &\quad+\int_0^1(\delta\tilde{\underline{\boldsymbol{\Lambda}}})\cdot\left[\left(\boldsymbol{W}_\zeta+\frac{(1-\zeta)\dot{R}_1}{R_1}\boldsymbol{\kappa}_\zeta\right)\right.\\ &\quad\left.\times\underline{\boldsymbol{J}}_\rho\cdot\left(\boldsymbol{W}_\zeta+\frac{(1-\zeta)\dot{R}_1}{R_1}\boldsymbol{\kappa}_\zeta\right)\right]\cdot\boldsymbol{\vartheta}d\zeta\\ &\quad-\int_0^1(\delta\tilde{\underline{\boldsymbol{\Lambda}}})\cdot\left[\underline{\boldsymbol{J}}_\rho\cdot\left(\frac{(1-\zeta)^2\dot{R}_1^2}{R_1^2}\boldsymbol{\kappa}_\zeta\right)\right]\cdot\boldsymbol{\vartheta}'\;d\zeta\\ &= \int_0^1-\tilde{\underline{\boldsymbol{\Lambda}}}_{n+1}\cdot\text{asym}\left[\underline{\boldsymbol{J}}_\rho\cdot\left\{\mathring{\boldsymbol{W}}_\zeta+\frac{(1-\zeta)\dot{R}_1}{R_1}\right.\right.\\ &\quad\times(2\,\boldsymbol{W}'_\zeta+\boldsymbol{\kappa}_\zeta\times\boldsymbol{W}_\zeta)\\ &\quad\left.\left.+\frac{(1-\zeta)\ddot{R}_1}{R_1}\boldsymbol{\kappa}_\zeta\right\}-\frac{(1-\zeta)^2\dot{R}_1^2}{R_1^2}\left(\boldsymbol{\kappa}_\zeta\times\underline{\boldsymbol{J}}_\rho\cdot\boldsymbol{\kappa}_\zeta\right)\right]\\ &\quad\cdot\underline{\boldsymbol{\Lambda}}_n^T\cdot\underline{\boldsymbol{T}}(\boldsymbol{\tau}_n)\cdot\Delta\boldsymbol{\theta}_{n+1}\cdot\boldsymbol{\vartheta}\;d\zeta\\ &\quad+\int_0^1\tilde{\underline{\boldsymbol{\Lambda}}}_{n+1}\cdot\text{asym}\left[\underline{\boldsymbol{J}}_\rho\cdot\left(\frac{(1-\zeta)^2\dot{R}_1^2}{R_1^2}\boldsymbol{\kappa}_\zeta\right)\right]\\ &\quad\cdot\underline{\boldsymbol{\Lambda}}_n^T\cdot\underline{\boldsymbol{T}}(\boldsymbol{\tau}_n)\cdot\Delta\boldsymbol{\theta}_{n+1}\cdot\boldsymbol{\vartheta}'\;d\zeta\\ &\quad-\int_0^1\tilde{\underline{\boldsymbol{\Lambda}}}_{n+1}\cdot\text{asym}\left[\left(\boldsymbol{W}_\zeta+\frac{(1-\zeta)\dot{R}_1}{R_1}\boldsymbol{\kappa}_\zeta\right)\right.\\ &\quad\left.\times\underline{\boldsymbol{J}}_\rho\cdot\left(\boldsymbol{W}_\zeta+\frac{(1-\zeta)\dot{R}_1}{R_1}\boldsymbol{\kappa}_\zeta\right)\right]\\ &\quad\cdot\underline{\boldsymbol{\Lambda}}_n^T\cdot\underline{\boldsymbol{T}}(\boldsymbol{\tau}_n)\cdot\Delta\boldsymbol{\theta}_{n+1}\cdot\boldsymbol{\vartheta}\;d\zeta\,. \end{aligned}\tag{C.4}$$

Appendix D. Method to find $\boldsymbol{\chi}$ given $\underline{\boldsymbol{\Lambda}}$

Here, given a rotation tensor $\underline{\boldsymbol{\Lambda}}$ we find the vector $\boldsymbol{\chi}$ such that $\underline{\boldsymbol{\Lambda}}=\exp\{\text{asym}(\boldsymbol{\chi})\}$. We first note that (Argyris, 1982)

$$\exp\{\text{asym}(\boldsymbol{\chi})\}=\underline{\boldsymbol{I}}+\frac{\sin(|\boldsymbol{\chi}|)}{|\boldsymbol{\chi}|}\text{asym}(\boldsymbol{\chi})+\frac{1-\cos(|\boldsymbol{\chi}|)}{|\boldsymbol{\chi}|^2}\text{asym}(\boldsymbol{\chi})^2,\tag{D.1}$$

where $\underline{\boldsymbol{I}}$ is the identity tensor. We define $\underline{\boldsymbol{F}}=\text{asym}(\boldsymbol{\chi})/|\boldsymbol{\chi}|$, so that

$$\underline{\boldsymbol{\Lambda}}=\underline{\boldsymbol{I}}+\sin(|\boldsymbol{\chi}|)\underline{\boldsymbol{F}}+(1-\cos(|\boldsymbol{\chi}|))\underline{\boldsymbol{F}}^2.\tag{D.2}$$

Inverting the above, we find

$$\frac{1-\cos(|\boldsymbol{\chi}|)}{\sin(|\boldsymbol{\chi}|)}\underline{\boldsymbol{F}}=(\underline{\boldsymbol{I}}+\underline{\boldsymbol{\Lambda}})^{-1}(\underline{\boldsymbol{\Lambda}}-\underline{\boldsymbol{I}})=:\underline{\boldsymbol{R}}.\tag{D.3}$$

From the above we can easily show that

$$|\text{axial}(\underline{\boldsymbol{R}})|=\frac{1-\cos(|\boldsymbol{\chi}|)}{\sin(|\boldsymbol{\chi}|)}\quad\text{and}\quad\frac{\text{axial}(\underline{\boldsymbol{R}})}{|\text{axial}(\underline{\boldsymbol{R}})|}=\text{axial}(\underline{\boldsymbol{F}})=\frac{\boldsymbol{\chi}}{|\boldsymbol{\chi}|}\,.\tag{D.4}$$

Given $\underline{\boldsymbol{\Lambda}}$ we can compute $\underline{\boldsymbol{R}}$ and the above equations can then be solved to find $\boldsymbol{\chi}$. Note that if $\boldsymbol{\chi}$ is a solution then $(\frac{|\boldsymbol{\chi}|+2\pi}{|\boldsymbol{\chi}|})\boldsymbol{\chi}$ is also a solution. Therefore, for uniqueness of the solution we solve for $-\pi<|\boldsymbol{\chi}|\le\pi$.

References

Antman, S.S., 1974. Kirchhoffs problem for nonlinearly elastic rods. Q. Appl. Math. 32 (3), 221–240.

Argyris, J., 1982. An excursion into large rotations. Comput. Method Appl. M. 32 (1–3), 85–155.

Cao, D.Q., Liu, D., Wang, C.H.-T., 2006. Three-dimensional nonlinear dynamics of slender structures: cosserat rod element approach. Int. J. Solids Struct. 43 (3–4), 760–783.

Friedmann, P.P., Glaz, B., Palacios, R., 2009. A moderate deflection composite helicopter rotor blade model with an improved cross-sectional analysis. Int. J. Solids Struct. 46 (10), 2186–2200.

Gerstmayr, J., Dorninger, A., Eder, R., Gruber, P., Reischl, D., Saxinger, M., Schörgenhumer, M., Humer, A., Nachbagauer, K., Pechstein, A., et al., 2013. Hotint: A script language based framework for the simulation of multibody dynamics systems. In: ASME 2013 International Design Engineering Technical Conferences and Computers and Information in Engineering Conference. ASME. V07BT10A047–V07BT10A047

Green, A.E., Naghdi, P.M., Wenner, M.L., 1974. On the theory of rods II. developments by direct approach. Proc. R. Soc. Lond. A 337 (1611), 485–507.

Hilber, H.M., Hughes, T.J.R., Taylor, R.L., 1977. Improved numerical dissipation for time integration algorithms in structural dynamics. Earthq. Eng. Struct. D. 5 (3), 283–292.

Humer, A., 2013. Dynamic modeling of beams with non-material, deformation-dependent boundary conditions. J. Sound Vib. 332 (3), 622–641.

Ibrahimbegović, A., 1995. On finite element implementation of geometrically nonlinear reissner's beam theory: three-dimensional curved beam elements. Comput. Method Appl. M. 122 (1–2), 11–26.

Liu, L., Lu, N., 2016. Variational formulations, instabilities and critical loadings of space curved beams. Int. J. Solid. Struct. 87, 48–60.

McRobie, F.A., Lasenby, J., 1999. Simo–vu quoc rods using clifford algebra. Int. J. Numer. Meth. Eng. 45 (4), 377–398.

Newmark, N.M., 1959. A method of computation for structural dynamics. J. Eng. Mech. 85 (3), 67–94.

Reissner, E., 1973. On one-dimensional large-displacement finite-strain beam theory. Stud. Appl. Math. 52 (2), 87–95.

Roy, A., Chatterjee, A., 2009. Vibrations of a beam in variable contact with a flat surface. J. Vib. Acoust. 131 (4), 041010.

Rubin, M.B., 2001. Numerical solution procedures for nonlinear elastic rods using the theory of a cosserat point. Int. J. Solid. Struct. 38 (24–25), 4395–4437.

Simo, J.C., 1985. A finite strain beam formulation. the three-dimensional dynamic problem. part i. Comput. Method Appl. M. 49 (1), 55–70.

Simo, J.C., Vu-Quoc, L., 1986. A three-dimensional finite-strain rod model. part II: computational aspects. Comput. Method Appl. M. 58 (1), 79–116.

Simo, J.C., Vu-Quoc, L., 1988. On the dynamics in space of rods undergoing large motionsa geometrically exact approach. Comput. Method Appl. M. 66 (2), 125–161.

Singh, N., 2018. Dynamics of Axially Shortening and Lengthening Geometrically Exact Beams in 3-Dimensions. Indian Institute of Technology Kanpur.

Steinbrecher, I., Humer, A., Vu-Quoc, L., 2017. On the numerical modeling of sliding beams: a comparison of different approaches. J. Sound Vib. 408, 270–290.

Vu-Quoc, L., 1986. Dynamics of flexible structures performing large overall motions: a geometrically- nonlinear approach. Technical Report. EECS Department, University of California, Berkeley.

Vu-Quoc, L., Li, S., 1995. Dynamics of sliding geometrically-exact beams: large angle maneuver and parametric resonance. Comput. Method Appl. M. 120 (1–2), 65–118.

Vu-Quoc, L., Simo, J.C., 1987. Dynamics of earth-orbiting flexible satellites with multibody components. J Guid Control Dynam. 10 (6), 549–558.